Review paper

The role of *SLC12A* family of cation-chloride cotransporters and drug discovery methodologies

Shiyao Zhang [a, 1], Nur Farah Meor Azlan [b, 1], Sunday Solomon Josiah [b], Jing Zhou [c], Xiaoxia Zhou [a], Lingjun Jie [a], Yanhui Zhang [a], Cuilian Dai [a], Dong Liang [d], Peifeng Li [e], Zhengqiu Li [f], Zhen Wang [g], Yun Wang [c], Ke Ding [g, ***], Yan Wang [a, **], Jinwei Zhang [a, b, g, *]

[a] *Xiamen Cardiovascular Hospital of Xiamen University, School of Medicine, Xiamen University, Xiamen, Fujian, 363001, China*
[b] *Institute of Biomedical and Clinical Sciences, Medical School, Faculty of Health and Life Sciences, University of Exeter, Exeter, EX4 4PS, UK*
[c] *Department of Neurology, Institutes of Brain Science, State Key Laboratory of Medical Neurobiology and MOE Frontiers Center for Brain Science, Institute of Biological Science, Zhongshan Hospital, Fudan University, Shanghai, 200032, China*
[d] *Aurora Discovery Inc., Foshan, Guangdong, 528300, China*
[e] *Institute for Translational Medicine, Qingdao University, Qingdao, Shandong, 266021, China*
[f] *School of Pharmacy, Jinan University, Guangzhou, 510632, China*
[g] *State Key Laboratory of Chemical Biology, Research Center of Chemical Kinomics, Shanghai Institute of Organic Chemistry, Chinese Academy of Sciences, Shanghai, 200032, China*

ARTICLE INFO

ABSTRACT

The *solute carrier family 12* (*SLC12*) of cation-chloride cotransporters (CCCs) comprises potassium chloride cotransporters (KCCs, e.g. KCC1, KCC2, KCC3, and KCC4)-mediated Cl^- extrusion, and sodium potassium chloride cotransporters (N[K]CCs, NKCC1, NKCC2, and NCC)-mediated Cl^- loading. The CCCs play vital roles in cell volume regulation and ion homeostasis. Gain-of-function or loss-of-function of these ion transporters can cause diseases in many tissues. In recent years, there have been considerable advances in our understanding of CCCs' control mechanisms in cell volume regulations, with many techniques developed in studying the functions and activities of CCCs. Classic approaches to directly measure CCC activity involve assays that measure the transport of potassium substitutes through the CCCs. These techniques include the ammonium pulse technique, radioactive or nonradioactive rubidium ion uptake-assay, and thallium ion-uptake assay. CCCs' activity can also be indirectly observed by measuring γ-aminobutyric acid (GABA) activity with patch-clamp electrophysiology and intracellular chloride concentration with sensitive microelectrodes, radiotracer $^{36}Cl^-$, and fluorescent dyes. Other techniques include directly looking at kinase regulatory sites phosphorylation, flame photometry, $^{22}Na^+$ uptake assay, structural biology, molecular modeling, and high-throughput drug screening. This review summarizes the role of CCCs in genetic disorders and cell volume regulation, current methods applied in studying CCCs biology, and compounds developed that directly or indirectly target the CCCs for disease treatments.

1. Introduction

Transmembrane proteins such as pumps, channels, and transporters are vital components of living cells, facilitating the movement of ions or small molecules across the cellular membrane. This is crucial for the normal physiological function of systems such as the cardiovascular, kidney, and nervous systems. Over 406 potential ion channels and 533 extracellular transporter proteins have been identified by the Human Genome Project [1]. Nonetheless, only a small fraction of these proteins has been thoroughly examined. Among the 667 human protein efficacy targets and 189 pathogen protein efficacy targets identified for U.S. Food and Drug Administration (FDA)-approved drugs, a significant proportion, approximately 18%–19%, are ion channels/transporters [2]. This underscores the critical role that ion channels/transporters play in the treatment of diseases.

The members of the *solute carrier family 12* (*SLC12*) are transporters that are coupled with sodium and/or potassium, playing a role in the movement of chloride ions across various tissues, particularly in the kidney and choroid plexus of the brain [3]. The sensitivity of these transporters to inhibitors and/or activators is a crucial parameter that determines their functional characteristics. The existence of multiple genes with similar transport functions, but distinct roles due to tissue-specific expression, underscores the necessity for the development of novel research tools and therapeutic agents. This review article aims to emphasize the genetics, physiology, and pathology of *SLC12* family transporters, elucidate their control mechanisms in regulating cell volume, detail the available methodologies for studying their structure, function, and activity, and provide an overview of recent initiatives in drug discovery.

2. Overview of cation-chloride cotransporters

The *SLC12* family encodes the cation-chloride cotransporters (CCCs) and contains nine members (*SCL12A1–9*, Fig. 1). *SLC12A1–A3* encodes for a Na^+ dependent branch for Cl^- influx, which comprises two Na^+-K^+-$2Cl^-$ cotransporters (NKCC1 and NKCC2) and one Na^+-Cl^- cotransporter (NCC). *SLC12A4–A7* encodes four K^+ dependent branches for Cl^- efflux, which comprise four K^+-Cl^- cotransporters (KCC1–4). *SLC12A8* and *SLC12A9* represent two orphan members, and amino acid similarities are as low as 19% compared to other *SLC12A1–A7* members. *SLC12A8* encodes the polyamine transporter (CCC9) and was recently found to be a nicotinamide mononucleotide (NMN) transporter [4]. A recent demonstration has shown the existence of a functional link between the lateral hypothalamus and skeletal muscle via *SLC12A8*, with implications for sarcopenia and frailty [5]. *SLC12A9* encodes CCC interacting protein (CIP1), which may play a role in modifying the activity or kinetics of CCCs through heterodimer formation [6]. Recently, significant research progress has been made in the field of CCCs in structural biology, including NKCC1 [7,8], NKCC2 [9,10], KCC1 [11], KCC2 [12,13], KCC3 [12,13], and KCC4 [13,14]. These studies have preliminarily elucidated that NKCC1 simultaneously transports Na^+, K^+, and Cl^- ions in a 1:1:2 ratio [7], while KCC1–4 simultaneously transport K^+ and Cl^- ions in a 1:1 ratio [11]. Therefore, these studies confirm that the transport of K^+, Cl^-, and/or Na^+ on the cell membrane is facilitated by CCCs in an electroneutral manner.

2.1. Genetics and distributions of CCCs

There is differential expression of *SLC12A* family members in various human organs and tissues, as shown in Fig. S1 and
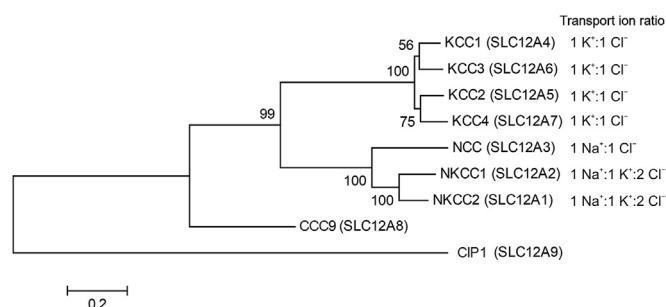
summarized in Table 1 [6,15–64]. Dysfunction of the *SLC12A* family members is linked to diseases and organ dysfunction. In mammalian kidneys, NKCC2 is expressed in the apical membrane and sub-apical cytosol of the thick ascending limb (TAL) [65]. Bartter syndrome type I (Online Mendelian Inheritance in Man (OMIM) database accession No.: OMIM 241200) is caused by inactivating mutations of NKCC2 in humans, and arterial hypotension is a significant characteristic of this condition [66]. NKCC1 is ubiquitously expressed in many cell types. In epithelial cells, NKCC1 is located in the basolateral membrane to supply Cl^- ions that will be secreted at the apical side of the cell [67]. In non-epithelial cells, NKCC1 plays an important role in the regulation of cell volume. The complete absence of NKCC1 expression in a human patient leads to hearing loss, intellectual disability, respiratory weakness, and the presence of mucus plugs [26]. The NCC protein is primarily located in the first segment of the distal convoluted tubule (DCT) in the kidney of mammals. Gitelman syndrome (OMIM 263800) is a salt-wasting disorder characterized by autosomal recessive inheritance and is commonly associated with loss-of-function mutations in *SLC12A3*, which encodes NCC [68]. The KCC1 protein is present in all tissues and is believed to have a significant function in controlling cell volume. In a study involving a humanized mouse model of sickle cell disease, it was observed that the KCC1 (M935K) mutant mice displayed heightened KCC1 activity, which caused extensive sickling of cells and tissue damage, ultimately leading to untimely death [69]. The expression of KCC2 is limited to neurons found in the central nervous system (CNS) [51] and retina [70], which play important roles in neuronal excitability [71], neuronal development [72], and circadian rhythm [73]. Loss of function mutations of KCC2 and altered expression levels both result in raised $[Cl^-]_i$ and compromised synaptic inhibition, and have been associated with cases of infantile epilepsy [44,45], idiopathic epilepsy [46,47], and acquired epilepsy [48]. According to two recent studies, KCC2 has been detected in INS-1E β-cell lines and glucagon-positive α cells located in pancreatic islets, and it plays a role in regulating insulin secretion [74,75]. KCC3 is also abundantly expressed and important in the regulation of cell volume. Numerous loss-of-function mutations in KCC3 have been identified and are linked to a medical condition known as hereditary motor and sensory neuropathy with agenesis of the corpus callosum (HMSN/ACC, OMIM#218000) [76,77], or Andermann syndrome, which is an autosomal recessive disorder that is marked by gradual sensory-motor polyneuropathy and partial or complete agenesis of the corpus callosum [78]. The development of peripheral motor neuropathy is associated with an atypical gain-of-function mutation in KCC3, suggesting that any unintended bidirectional shift in KCC3 function can impact the physiology of the peripheral nerves [54]. KCC4 is also extensively expressed and may play a significant role in the cotransport of K^+ and Cl^- in the kidneys. Mice that lack KCC4 exhibit symptoms of renal tubular acidosis and deafness [79]. The expression of CCC9 is highly abundant in intracellular compartments, and it is believed to aid in the transportation of polyamines and amino acids across the cell surface [80]. It has been discovered that CCC9 is the first NMN transporter and plays a crucial part in the regulation of nicotinamide adenine dinucleotide metabolism in the intestines [4]. CIP1 is present in various tissues, such as the placenta, brain, and kidney, and it is expressed at elevated levels [6]. CIP1 is also ubiquitously expressed during the postnatal development of rats [81]. CIP1 inhibits the functional expression of co-expressed NKCC1 [6] and interacts with KCC2 to increase its activity [81], but the specific substrate that CIP1 transports remains unknown.

2.2. Dysregulation of CCCs family in disease conditions

Dysregulation of CCC expression and function has been implicated in various disease conditions, including neurological

Fig. 1. Phylogenetic tree of the *solute carrier family 12* (*SLC12*) family of cation-chloride cotransporters (CCCs) in humans. The *SLC12* family's phylogenetic tree was constructed using MEGA package via the neighbor-joining method. For reliable tree topologies, 1,000 bootstrap analysis trials were conducted. Branch length represents the average amino acid substitutions per site. The scale bar indicates 0.2 substitutions per site. KCC: K^+-Cl^- cotransporter; NCC: Na^+-Cl^- cotransporter; NKCC: Na^+-K^+-$2Cl^-$ cotransporter; CIP: CCC interacting protein.

Table 1
Solute carrier family 12 (SLC12) family of cation-chloride cotransporters (CCCs) in human disorders.

Human gene name	Protein name	Transport type/coupling ions	Tissue and subcellular distribution	Genetic mutations link to human diseases	Year of gene cloning and characterization
SLC12A1	NKCC2	Cotransport/Na$^+$/K$^+$/2Cl$^-$	Kidney-specific: located on the apical membrane of the thick ascending limb (TAL); hypothalamo-neurohypophyseal system	Gene defect: many cases in Bartter's syndrome; rare cases in growth abnormality [15], developmental disorder [16], nephrocalcinosis, and hypercalciuria [17]	1994 [18,19]
SLC12A2	NKCC1	Cotransport/Na$^+$/K$^+$/2Cl$^-$	Ubiquitous; basolateral plasma membrane	Autism [20–22], schizophrenia [23,24], developmental disorder [16,20], intellectual disability [20,22,25], Kilquist syndrome [26], encephalopathy syndrome [27], hearing loss [28–30], and congenital heart defect [31]	1994 [32,33]
SLC12A3	NCC	Cotransport/Na$^+$/Cl$^-$	Kidney-specific: located on the apical membrane of the distal convoluted tubule (DCT); bone	Gene defect: many cases in Gitelman syndromes; and rare cases in short stature [34], or diabetic nephropathy [35,36]	1993 [37]
SLC12A4	KCC1	Cotransport/K$^+$/Cl$^-$	Ubiquitous	Autism spectrum disorder [16,38,39], ovarian carcinoma [40], red blood cell traits [41], and high-density lipoprotein cholesterol [42]	1996 [43]
SLC12A5	KCC2	Cotransport/K$^+$/Cl$^-$	Neuron-specific; located on the basolateral plasma membrane; retina; pancreatic islets or INS-1E β-cell lines	Infantile epilepsy [44,45], idiopathic epilepsy [46,47], acquired epilepsy [48], autism spectrum disorder [49,50], and schizophrenia [50]	1996 [51]
SLC12A6	KCC3	Cotransport/K$^+$/Cl$^-$	Ubiquitous	Agenesis of the corpus callosum with peripheral neuropathy [52–54], andermann syndrome [55], and agenesis of corpus callosum [56,57]	1999 [58–60]
SLC12A7	KCC4	Cotransport/K$^+$/Cl$^-$	Ubiquitous; basolateral plasma membrane	Developmental disorder [16], developmental and epileptic encephalopathy [61], and hydrocephalus [62]	1999 [60]
SLC12A8	CCC9	Nicotinamide and mononucleotide	Ubiquitous		2002 [63]
SLC12A9	CIP1	Unknown	Ubiquitous	Developmental disorder [16], congenital heart disease [64], and autism spectrum disorder [16,38]	2000 [6]

NKCC: Na$^+$-K$^+$-2Cl$^-$ cotransporter; NCC: Na$^+$-Cl$^-$ cotransporter; KCC: K$^+$-Cl$^-$ cotransporter; CCC: cation-chloride cotransporter; CIP1: CCC interacting protein.

conditions, cardiovascular diseases (CVDs), and certain types of cancer.

2.2.1. KCC2 and NKCC1 in neurological conditions

In the adult brain, KCC2 creates a chloride electrochemical gradient that moves inwardly and results in hyperpolarizing responses mediated by γ-aminobutyric acid subtype A (GABA$_A$) receptors (GABA$_A$Rs) [82]. There have been reports of GABA exhibiting depolarizing or even excitatory effects. The decrease in KCC2 expression could be a contributing factor to the depolarizing or excitatory effects of GABA. KCC2 expression is limited after birth, particularly in the hippocampus and cortex, and gradually increases over the first two weeks until it attains adult levels [72]. Impaired KCC2 expression and function, resulting in raised [Cl$^-$]$_i$ and compromised synaptic inhibition, has been linked to various types of epilepsy [44–48], autism [83], pain [84], and Rett syndrome [85]. Under ischemic conditions, a reduction in KCC2 expression was noticed in hippocampal slices, particularly following oxygen-glucose deprivation [86], as well as in an in vivo model of global ischemia [87]. In contrast, upregulation of NKCC1 promotes chloride ion influx, which leads to neuronal hyperexcitability and seizure activity, etc.. NKCC1 upregulation was observed in rodents with neonatal seizures [88], temporal lobe epilepsy [89], neuroinflammation [90], cerebral stroke [91], post-hemorrhagic hydrocephalus [92], traumatic brain injury [93], paclitaxel-induced neuropathic pain (NP) [94], and NP induced by spinal cord injury [95]. It can be inferred from all of this that activating KCC2 activity or inhibiting NKCC1 activity could have advantageous effects in treating these neurological conditions.

2.2.2. CCCs in CVDs
2.2.2.1. NKCC1 and KCCs in vascular cells.
An increase in NKCC1 activity was detected in the aorta of rats with streptozotocin-induced diabetes [96], and in the left ventricle of db/db mice when compared to their wild-type counterparts following cardioplegia-induced arrest [97]. Both genetic and pharmacological evidence suggests that reduced NKCC1 activity inhibits cell contractile responses in vascular smooth muscle cells (VSMCs) [98]. The presence of the messenger RNAs (mRNAs) of KCC1 and KCC3 was discovered in primary cultures of VSMCs by specific reverse transcription-polymerase chain reaction (PCR) analysis, while KCC2 mRNA was found at extremely low levels, and KCC4 mRNA was not detectable [99]. The inactivation of KCC3 in a mouse model resulted in an increase in systemic vascular resistance and ventricular mass, as well as the prevention of extracellular fluid volume accumulation [100]. The acute upregulation of KCC3 mRNA expression in primary cultures of rat VSMCs is induced by the fast nitric oxide (NO) releasers NOC-9 and NOC-5, and it is dependent on NO/soluble guanylyl cyclase signaling [101]. Platelet-derived growth factor was found to mediate a time-dependent increase in KCC1 mRNA expression and a decrease in KCC3 mRNA expression in rat VSMCs [102].

2.2.2.2. NKCC2 and NCC in renal cells.
Patients with Gordon's syndrome or pseudohypoaldosteronism type II (PHAII) exhibit altered renal NaCl handling and blood pressure due to enhanced expression

and activity of NCC and NKCC2 resulting from gain-of-function mutations in with-no-lysine (K) kinases (WNKs), and their upstream ubiquitin E3 ligase components Cullin-3 (CUL3) and Kelchlike 3 (KLHL3) [103,104]. PHAII is a condition that presents with symptoms such as hyperkalemia, metabolic acidosis, hypertension, and either low or normal plasma renin activity and aldosterone concentration. According to mouse models, the gain-of-function mutations of WNKs, CUL3, or KLHL3, resulting in increased activating phosphorylation of NCC and NKCC2, cause hypertension in individuals with PHAII [105–108]. Both genetic and pharmacological evidence suggests that reducing NCC or NKCC2 activities directly or indirectly benefits renal sodium homeostasis and blood pressure normalization in human patients or animal models [109,110]. These findings suggest that decreasing the activity of NKCC2, NKCC1, and NCC, or increasing KCC activity, could be beneficial in the context of CVDs. For further details, refer to our previous review [111].

2.2.3. CCCs in cancer

CCCs have been linked to the development and progression of cancer. Overexpression of NKCC1 in mice fibroblasts has been shown to trigger cell proliferation and morphological changes [112]. Accumulating evidence suggests a strong association between the expression of NKCC1 protein and tumor progressions, including lung adenocarcinoma [113], cells of gastric cancer [114], and prostate cancer cells [115]. Additionally, Shiozaki et al. [116] suggested that NKCC1 appears to have a significant impact on the advancement of the cell cycle in cases of human esophageal squamous cell carcinomas. Luo et al. [117] found that both the mRNA and protein of NKCC1 were expressed at high levels in gliomas of all grades. All these findings suggest that increased expression of NKCC1 is linked to higher rates of cell proliferation and invasiveness, and inhibiting NKCC1 may have therapeutic benefits in treating cancer. After treatment with insulin-like growth factor-2, cervical cancer cells exhibited a marked increase in both KCC1 mRNA and protein expression [118]. An in vivo study demonstrated that enhanced KCC1 activity exacerbates end-organ damage and decreases survival rates in individuals with sickle cell disease [69]. KCC1 has been shown to operate as a chloride extruder in mouse osteoclasts, where it performs a critical function in the extrusion of H^+ during bone resorption [119]. The expression of KCC3 is increased by insulin-like growth factor-1, promoting cell growth, while it is decreased by tumor necrosis factor-alpha, resulting in growth arrest [120]. Disabling both erythroid KCC1 and KCC3 causes changes in erythrocyte volume and can partially alleviate erythrocyte dehydration in seasonal affective disorder (SAD) mice [121]. This suggests that KCC1 and KCC3 play important supporting roles in cancer cells and provide potential therapeutic options.

3. Methods for studying *SLC12* family members the functions and activities

3.1. Cell volume regulation

Both the intracellular and extracellular fluids contain a wealth of inorganic salt ions, and normal cells regulate cell volume by transporting ions across the cell membrane. When the physical or chemical properties of the extracellular fluid are disrupted, such as changes in osmotic pressure causing cell swelling or shrinkage, most cells activate specialized membrane channels to counter the disturbance. This helps restore the environment that had been affected, enabling the cell to return to its normal state. The CCCs of *SLC12* family are crucial for maintaining proper cell volume regulation. These transporters sense both osmotic pressure and

intracellular chloride concentration ($[Cl^-]_i$), which is essential for regulating cell volume [122,123]. During cells experience acute shrinkage, they are regulated by a process known as regulatory volume increase (RVI). Likewise, when cells undergo acute swelling, they are regulated by regulatory volume decrease (RVD).

RVI typically occurs when cells are exposed to hypertonic fluid after being in isotonic fluid or when they are exposed to hypotonic fluid for a certain duration before entering isotonic fluid. The second condition occurs after RVD and is known as post-RVD RVI [124]. The process of RVI primarily relies on cotransporters such as NKCC1 or NKCC2 [125], NCC, Na^+-H^+ exchanger [126], Cl^--HCO_3^- anion exchanger [127], and Na^+ channels [128] present in the cell membrane to facilitate ion exchange in response to acute cell shrinkage. Upon cell shrinkage, NKCCs and NCCs are rapidly activated, allowing Na^+, K^+, and Cl^- to move into the cell, thereby restoring the original cell volume [129]. The post-RVD RVI (or RVD-after-RVI) process occurs when cells undergo hypotonic adaptation and enter isotonic fluid, creating a relatively hyperosmotic state. This may happen because the reduced intracellular concentration of Cl^- during the previous RVD process makes the NKCCs more sensitive to cell shrinkage stimuli. On one hand, RVD typically occurs when cells are exposed to a hypotonic solution from an isotonic solution or when they are pre-adapted to hypertonic fluid for a while before entering isotonic fluid. The latter condition occurs after RVI and is also known as post-RVI RVD (or RVI-after-RVD) [124]. On the other hand, the process of RVD mainly depends on KCCs [130], K^+ channels [131], and Cl^- channels [132] in the cell membrane to accomplish ion exchange in response to acute cell swelling. These membrane transporters are rapidly activated when the cell swells, and KCC activation leads to a decrease in cell volume through K^+ and Cl^- efflux, with the final volume returning to slightly higher initial values [133]. A detailed summary of ion transport and cell volume changes during RVI and RVD is provided in Figs. 2 and 3 and Table S1.

The CCCs family can modulate cell volume homeostasis through their direct phosphorylation or dephosphorylation [134]. The WNK kinase family and its downstream STE20 family are capable of directly regulating ion channels and cotransport proteins such as NKCCs, NCCs, and KCCs in the cell membrane. In response to cell shrinkage, the activity of WNKs and SPS/Ste20-related proline-alanine-rich kinase (SPAK)/oxidative stress-responsive kinase 1 (OSR1) increases, leading to the activation of NKCCs following phosphorylation and inhibition of KCCs [135]. Conversely, when cells swell, WNKs and SPAK/OSR1 are inactive, causing KCCs to be activated via dephosphorylation and NKCCs to be inhibited [130]. This suggests that the kinase-active WNK family regulates cellular osmolarity and intracellular chloride homeostasis by promoting Cl^- influx through NKCCs and inhibiting Cl^- efflux through KCCs [136]. A recent exciting discovery by Boyd-Shiwarski et al. [137] suggests that WNK kinases use phase separation, mediated by their intrinsically disordered C-terminal domain, to sense molecular crowding and activate RVI. This phosphorylation and dephosphorylation mechanism of this signaling pathway has been validated in several studies exploring brain edema complications caused by ischemic stroke or cerebral ischemia-reperfusion injury, effectively regulating the volume of neurons and oligodendrocytes [138]. The serine/threonine kinase p38 mitogen-activated protein kinase has long been known to be involved in the process of RVI in epithelial cells [139]. Surprisingly, it was recently discovered that p38 can phosphorylate and activate NKCC1 to participate in RVI and increase cell volume near the wound, thus accelerating wound healing [140]. Other protein kinases that have been found to regulate the activation or phosphorylation of CCCs include c-Jun N-terminal protein kinases [141]
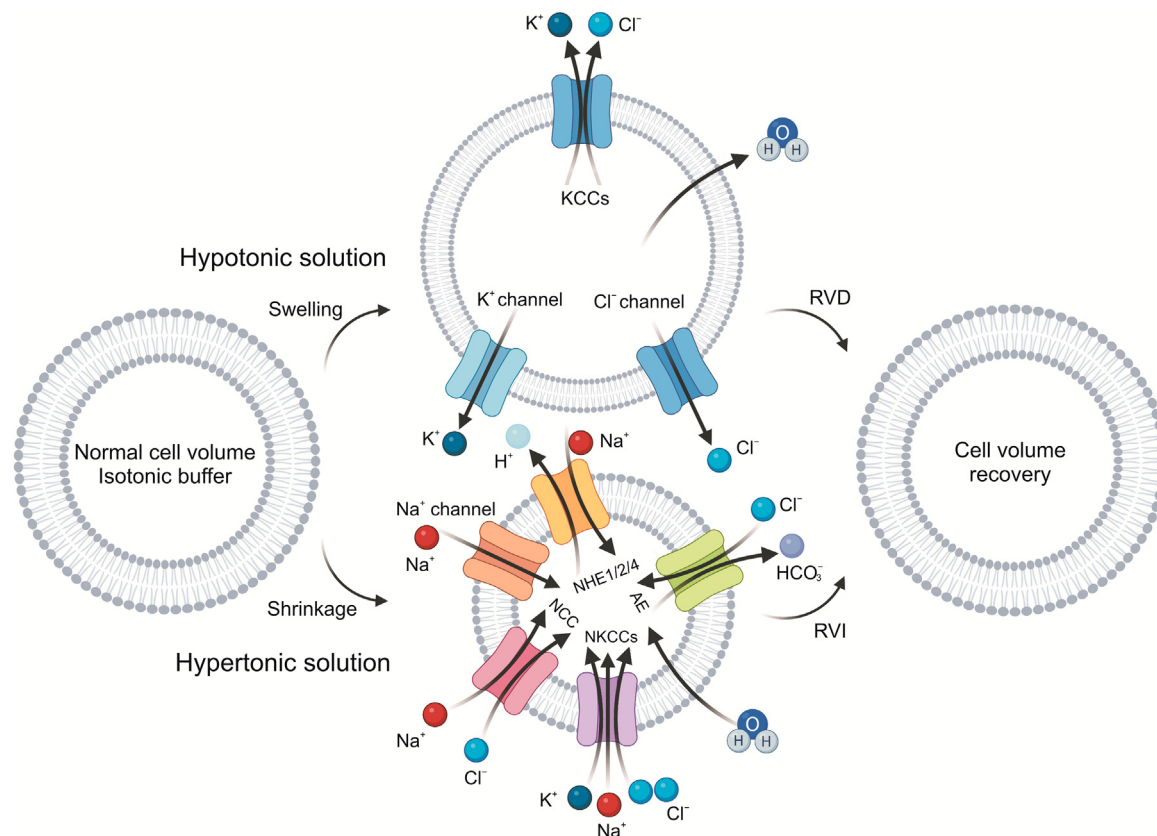
Fig. 2. Changes in cell volume resulting from the transport of Na^+, K^+, and Cl^- ions during regulatory volume increase (RVI) and regulatory volume decrease (RVD). Cell volume RVD in hypotonic fluid and shrinkage (RVI) in hypertonic fluid. RVD activates K^+-Cl^- cotransporters (KCCs), K^+ channels, and Cl^- channels, promoting ion and water efflux, reducing cell volume. RVI activates transporters (Na^+-K^+-$2Cl^-$ cotransporters (NKCCs), Na^+-Cl^- cotransporter (NCC), Na^+-H^+ exchanger (NHE), and Cl^--HCO_3^- anion exchanger (AE)) and Na^+ channels, inducing ion and water influx, increasing cell volume. RVI and RVD collaborate to restore the cell's original volume. The diagram was created using BioRender.com.

and myosin light chain kinase [142]. In addition to directly influencing the activity of CCCs transporters, the function of these transporters can also be indirectly influenced through several other transport mechanisms. NKCC1 has been found to form a complex with the Leu transporter, large amino acid transporter 1, which can inhibit its function and the protein kinase B/extracellular signal-regulated kinase pathway, leading to the inhibition of the mechanistic target of rapamycin complex 1 activation, thereby regulating cell volume [143]. Whether the CCCs family of transporters acts directly or indirectly, it is evident that they play an essential role in regulating cell volume and intracellular chloride concentration.

One commonly used method to observe changes in cell volume during RVI and RVD is the Coulter Counter Analyzer (Beckman), which measures electric conductance. This method is considered highly accurate and can detect particles as small as 0.1 μm in size. Before testing the sample cells, the cells are typically diluted, with the specific dilution dependent on their density. Generally, a cell density of 5,000 to 10,000 cells/mL volume is used. Baseline measurements are taken in the control medium, and measurements of the cells in the experimental group are taken at intervals to calculate the average volume of all cells. Cell volume changes are observed and compared to the baseline data [144]. Moreover, chloride ions are among the most abundant ions in the cell, and NKCCs, NCCs, and KCCs are involved in regulating cell volume in relation to Cl^-. The intracellular Cl^- concentration increases during RVI and decreases during RVD, serving as a volume sensor. Therefore, measuring Cl^- content using chemical chloride probes, such as *N*-(ethoxycarbonylmethyl)-6-methoxyquinolinium

bromide (MQAE), could reflect relative changes in cell volume and allow for quantitative analysis [145]. Cell size in the two-dimensional plane can also be estimated indirectly as cell volume. The length, width, and area of cells are measured by manually identifying the cell boundaries under the microscope. Assuming that the change in cell width and thickness is proportional, the relative cell volume is calculated using the formula $volume_t/volume_c = (area_t \times width_t)/(area_c \times width_c)$, where t and c in the formula refer to the test experimental group and the control group, respectively [146]. Other methods, such as succinimidyl ester staining, can mark the mass of intracellular proteins to reflect cell size [147].

3.2. Flame photometry

One traditional approach to directly examine the fluxes of K^+ and Na^+ involves measuring changes in the intracellular content of Na^+, K^+, and Cl^- using flame photometry. In this technique, solutions are drawn into an excitation region, and a high-temperature atomization source (flame) generates energy, which excites the atoms to higher energy levels. As the excited atoms return to the unexcited ground state, they emit light at a characteristic wavelength. A photocell is employed to detect the emitted light by converting it into a voltage. Since Na^+ and K^+ generate light of different wavelengths, appropriate filters allow for the simultaneous measurement of the emission produced by both Na^+ and K^+ in the same sample. The light absorption of the atoms in the flame is proportional to the ion concentration in the sample, allowing the calculation of element concentrations in the sample based on the
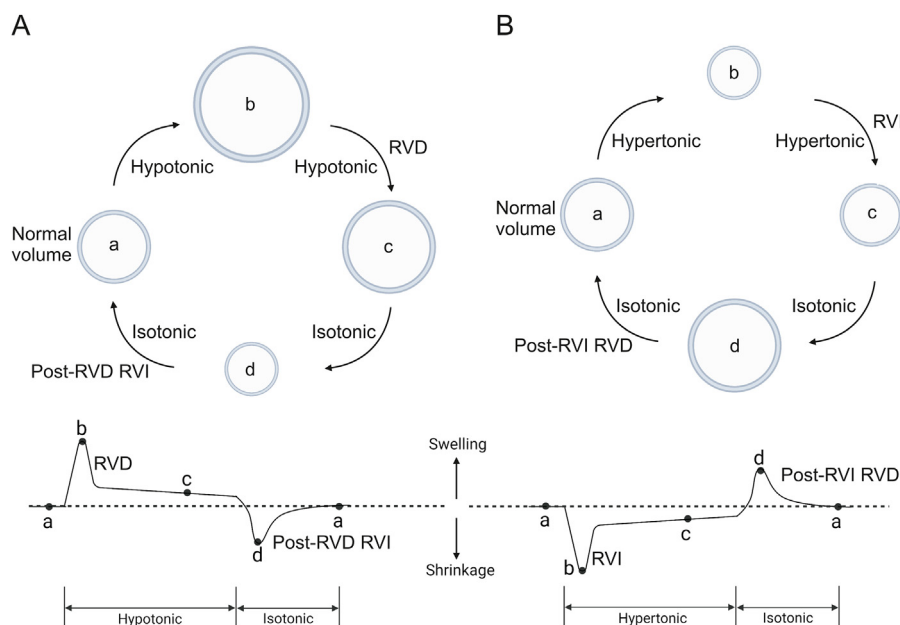
Fig. 3. The adjustment of cell volume in solutions with different osmotic pressures. (A) Cell volume changes occur during regulatory volume decrease (RVD) and post-RVD regulatory volume increase (RVI) processes in response to hypotonicity and return to isotonicity (a: normal volume; b: acute swelling in response to hypotonic stimulation; c: cell volume slightly higher than normal after RVD in hypotonic fluid; and d: RVI-after-RVD, where cells first shrink and then return to normal volume). (B) Cell volume changes in response to hypertonic conditions, activating RVI and post-RVI RVD mechanisms, followed by return to isotonicity (a: normal volume; b: acute shrinkage due to hyperosmolarity; c: cell volume slightly lower than normal after RVI in hypertonic fluid; and d: RVD-after-RVI, where cells first swell and then return to normal volume). The diagram was created using BioRender.com.

intensities of the absorbed wavelengths in relation to a reference standard [148]. Although this method effectively determined the stoichiometry of Na$^+$-K$^+$-Cl$^-$ (1:1:2) [149], flame photometers are intricate to use and relatively expensive. Moreover, they respond linearly to ion concentrations over a narrow concentration range, requiring the preparation of suitable dilutions.

3.3. $^{22}Na^+$ uptake assay

The conventional approach to investigating the thiazide or thiazide-like diuretic drug (such as metolazone)-sensitive NCC is through the measurement of the radioactive uptake of $^{22}Na^+$ by liquid scintillation (Section S1 in the Supplementary data) [135]. This method has been widely used in studies of NCC using *Xenopus laevis* oocytes [150], mammalian cell lines expressing native NCC [135], or mouse distal convoluted tubule cells that endogenously express NCC [151]. These studies have significantly improved our understanding of NCC regulation, especially regarding post-translation modifications such as phosphorylation [109], glycosylation [152], and ubiquitination [153]. Researchers have explored alternative methods due to the limited number of mammalian cell-based analyses and the hazards associated with using radioactive $^{22}Na^+$ [154], despite several attempts to enable NCC activity and localization in mammalian cell systems.

3.4. Radioactive rubidium ($^{86}Rb^+$) ion uptake assay

Assessing KCCs through the measurement of radioactive $^{86}Rb^+$ flux across the membrane of uniform cell preparations is a commonly employed method. Once the radioactive isotope passes through the channel, it acts as a tracer, allowing direct measurement of channel activity. The technique involves incubating cells in a Na$^+$/K$^+$-free solution to inhibit endogenous KCCs. This is followed by incubation with ouabain and an uptake medium containing

ouabain and $^{86}Rb^+$. After lysing the cells, tracer activity is measured using liquid scintillation counting. While this method is robust, highly sensitive, and selective, its applications are limited in tissues with multiple cell types, such as brain or neuron cultures. This limitation arises from the difficulty in distinguishing between channel activities in different cell types. Additionally, the approach cannot resolve ion concentration changes at the subcellular level. The use of a radioactive isotope with a short half-life (18.65 days) and high-energy emission (max 1.77 MeV; min 1.08 MeV) poses safety issues, making it particularly problematic when studying neuronal cells that require a high number of cells [155]. Nonetheless, this approach has contributed significantly to our understanding of KCC activity.

3.5. Ammonium pulse technique

To avoid the use of radio elements, researchers employ the ammonium pulse technique, also known as the NH$_4^+$ uptake assay. The principle underlying this assay is that both NKCCs and KCCs are capable of transporting NH$_4^+$, which serves as the basis for measurement [156]. The application of extracellular NH$_4^+$ induces NH$_4^+$ influx, resulting in biphasic changes in intracellular pH. Initially, the influx of NH$_3$ into the cell, caused by increased permeability of the cytoplasmic membrane to alkyl NH$_3$, leads to an increase in cellular pH. Second, there is a CCC-dependent decrease in cellular pH due to the CCC-mediated import of NH$_4^+$, which causes acidification. The intracellular pH can be monitored by using the pH-sensitive fluorescent dye 2′,7′-bis(2-carboxyethyl)-5(6)-carboxyfluorescein (BCECF) after inducing an alkaline load with NH$_4^+$. The rate of BCECF fluorescence quenching is used to measure NH$_4^+$ transport. The emitted fluorescence is detected using fluorescence microscopy at a wavelength of 530 nm [156]. The acidification in the presence of NH$_4$Cl is then extrapolated to CCC activity [157]. The elevation of intracellular pH is indicated by an

increase in fluorescence, which has been utilized by various research groups to investigate the activity of KCCs [158,159] and NKCCs [160−162]. While this real-time estimation approach enables the evaluation of CCC activity at a cellular and subcellular level, it has some limitations. Notably, KCC2 can induce reverse Cl$^-$ transport, leading to significant intracellular pH changes. Additionally, other transports, channels, and ion exchangers may influence intracellular pH changes, as reported [163].

3.6. Non-radioactive rubidium (^{85}Rb$^+$) ion uptake assay

In the late 1990s, Terstappen [155] developed the non-radioactive ^{85}Rb$^+$ efflux assay to replace the radioactive ^{85}Rb$^+$ assay for determining ion fluxes. Since its discovery, this method has become widely used in drug discovery and development and has largely replaced radioactive ^{86}Rb$^+$ assays for analyzing K$^+$ and nonselective cation channels in the pharmaceutical industry [155]. The non-radioactive ^{86}Rb$^+$ efflux assay comprises two primary stages: the manipulation and cultivation of cells, followed by the identification of the tracer rubidium using atomic absorption spectroscopy (AAS). As illustrated in Section S2 in the Supplementary data [130,155], the steps involved in the non-radioactive ^{85}Rb$^+$ efflux assay. First, cells expressing the ion channel under investigation are cultured in microplates, and tracer rubidium is loaded by exchanging potassium in a cell-compatible buffer solution with the same concentration of rubidium. This loading phase, typically lasting for 2−4 h, involves the pumping of ^{85}Rb$^+$ into the cells by cellular Na$^+$/K$^+$-ATPases. This process can be inhibited by the cardiac glycoside ouabain. Prior to conducting efflux experiments, excess RbCl is removed through rapid washes using an isotonic buffer depend on various factors such as cell type, cell density, microplate format, and the washing equipment used. Optimization of these steps is crucial for achieving favorable signal-to-background ratios and a distinct signal window [164]. Once the channel of interest is activated, ^{85}Rb$^+$ is released into the supernatant of the cells. The supernatant and the remaining cells are collected and analyzed using AAS to quantify the amount of rubidium. To calculate the ^{85}Rb$^+$ efflux, the proportion of rubidium present in the supernatant is measured relative to the total rubidium content, which includes both ^{85}Rb$^+$ in the supernatant and the cell lysate. This method eliminates variations in cell densities and losses that may occur during the assay process or ^{85}Rb$^+$ loading. While the method is user-friendly, it requires a series of assay validation experiments and may have suboptimal temporal resolution [165]. Despite its limitations, the non-radioactive ^{85}Rb$^+$ efflux assay remains a reliable method for evaluating KCCs and NKCCs [130].

3.7. Thallium ion (Tl$^+$) uptake assay

The Tl$^+$ flux assay employs Tl$^+$ as a substitute for K$^+$ since it has a strong affinity for the K$^+$ site present in KCCs and NKCCs (Fig. 4 and Sections S3 and S4 in the Supplementary data [130,155,165]). The entry of Tl$^+$ ions into cells can be detected by employing a Tl-sensitive fluorescent dye such as benzothiazole coumarin (BTC) or fluozin-2. When transported by the channel, Tl$^+$ ions may bind to the BTC/fluozin-2 dye, causing a fluorescent change that can be measured using a fluorometric imaging plate reader [155]. Tl$^+$ indicator dyes are introduced into cells as acetoxymethyl esters, which are subsequently cleaved by cytoplasmic esterase, releasing active fluorogenic forms. To activate the potassium-chloride transporter, cells are stimulated with a combination of K$^+$ and Tl$^+$ in the presence or absence of experimental compounds, such as NKCC1 inhibitors or KCC2 activators. As Tl enters the cell and binds to the fluorescence dye, the increase in fluorescent signal corresponds to the influx of Tl$^+$ ions into the cell via the cotransporter. Thus, it provides a functional measure of the cotransporter's activity.

The FluxOR dye is a novel fluorescent dye that is 10-fold more Tl sensitive than BTC [166]. Unlike BTC, this dye allows assessment in physiological saline with standard chloride concentrations [167]. This discovery led to the screening of multiple compounds using the fluozin-2 fluorescent dye [168]. The method successfully measured KCC2 and NKCC2 activity in different cell cultures, including HEK293 cells expressing human KCC2 [169], the renal epithelial LLC-PK1 cells transfected with NKCC2 [165], and Sf9 insect cells expressing mouse KCC2 (mKCC2) [170]. These cells were seeded in a 96-well plate with black walls and a clear bottom. However, it is important to consider that off-target pathways like the Na$^+$/K$^+$ ATPase in HEK293 cells may interfere with Tl$^+$ influx, potentially leading to false positives or false negatives [171]. Furthermore, this method is limited in neuronal cells due to their low viability following multiple washes. The presence of various K$^+$ channels and transporters in neurons also hinders precise evaluation of KCC2-mediated K$^+$ fluxes. The low temporal and spatial resolution of this approach further restricts investigation in small neuronal compartments, such as axons, dendrites, and dendritic spines.

3.8. Observing GABA activity with patch-clamp-electrophysiology

The basis for all electrophysiological measurements of KCC2 function is the permeability of GABA$_A$Rs to chloride ions. KCC2 is a significant modulator of inhibitory GABAergic activity, and its chloride extrusion activity is responsible for the hyperpolarization of GABA$_A$Rs. Intracellular recordings provide valuable information by extrapolating KCC2's chloride extrusion capacity from the reversal potential of GABA$_A$R-mediated currents (E_{GABA}). A lower intracellular chloride concentration, indicated by a hyperpolarized E_{GABA}, suggests an increase in KCC2 activity.

The gold standard approach for measuring ion channel activity in electrophysiology is the patch-clamp technique. This method involves creating a tight seal on the cell surface using a glass electrode with a relatively large bore. This allows for the recording of intracellular activity of ion channels in reference to another electrode in a bath surrounding the cell. This technique can be performed in two modes: voltage clamp mode, where the amount of current that crosses a cell's membrane is measured at a fixed voltage, or current clamp mode, where the amount of voltage moving across the membrane is recorded at a fixed current [172]. Various modifications of the fundamental patch-clamp technique can be employed, depending on the research objectives. The whole-cell mode (Fig. 5A) is the most prevalent patch-clamp configuration, which involves creating an electrical and molecular connection to the intracellular space by briefly applying intense suction to rupture the cell membrane surface.

This configuration records the currents through multiple channels simultaneously, which is useful for studying the real-time effect of drug treatment in cells. However, due to the difference in volume between the electrode and the cell, intracellular dialysis may occur, whereby the soluble contents of the cell interior are gradually replaced by the contents of the electrode. A similar, but improved, configuration is the perforated patch configuration (Fig. 5B and Section S5 in the Supplementary data [71,72]), in which electrode solution containing pore-forming antibiotics or antifungals such as gramicidin, nystatin, or amphotericin B is used to form small pores in the membrane, instead of using strong suction for cell rupture [172]. In particular, the introduction of gramicidin generates pores that selectively allow cations to pass through the
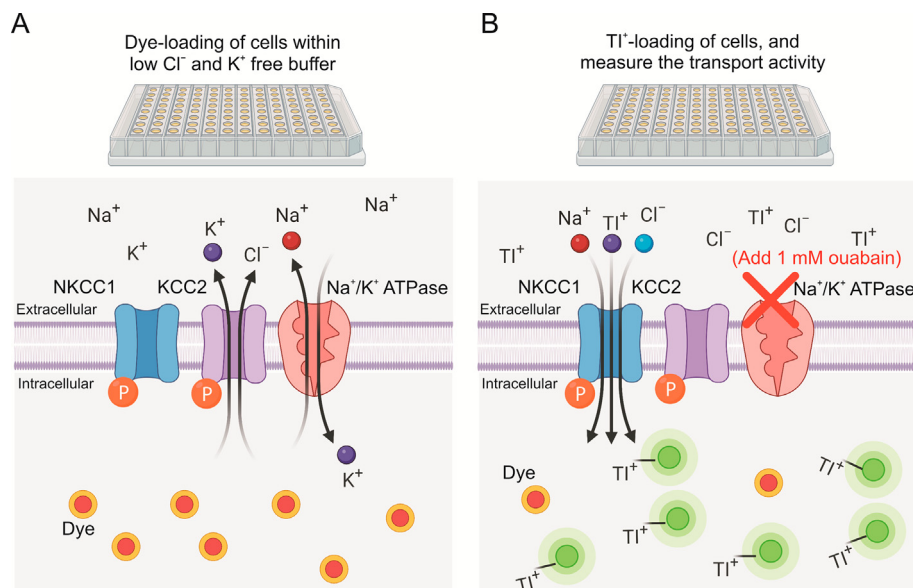
Fig. 4. Scheme of a thallium (TI) uptake assay to measure Na^+-K^+-$2Cl^-$ cotransporter 1 (NKCC1) or K^+-Cl^- cotransporter 2 (KCC2) activity. (A) Cells are pre-incubated with TI^+ sensitive dye FluxOR dye in a buffer with low Cl^- and low K^+ to promote NKCC1 activation or KCC2 inhibition. (B) For the assay, cells are incubated with the addition of TI^+ and Cl^-. NKCC1 or KCC2 operation leads to the absorption of TI^+ ions and an upsurge in the fluorescence of the TI^+-sensitive dye FluxOR. The addition of ouabain hinders the functioning of Na^+-K^+-ATPase. The diagram was created using BioRender.com.

membrane, with little to no permeability to anions. The gramicidin-perforated patch clamp technique has been employed by numerous researchers to evaluate the activity of KCC2 [173,174]. Many researchers have increasingly adopted the use of gramicidin-perforated patch clamp recordings as a means of studying the functions and activities of the *SLC12* family of CCCs in the context of evaluating or monitoring $[Cl^-]_i$ homeostasis [175–177].

The robustness of this technique has been confirmed by several studies. For instance, Ebihara et al. [178] examined the effect of GABA on neurons dissociated from the rat substantia nigra pars reticulata and found that no change in $[Cl^-]_i$. Another example, Lamsa et al. [179] used this technique to prevent unintended changes in membrane potential and E_{GABA} that may arise due to GABA$_A$R activation, leading to the opening of chloride and bicarbonate conductance. This was performed in both neonatal hippocampal cells and mature interneurons [179].

Kyrozis and Reichling [180] conducted a study to validate the stability of $[Cl^-]_i$ using this technique. They measured the responses of glycine and GABA receptors, which can gate chloride conductance, to their respective agonists. Their study confirmed that continuous electrical access through the perforated patch clamp technique does not cause significant modification of intracellular chloride concentration. As the electrode tip partially occupies the membrane, the current resolution is diminished and recording noise is more likely to occur. The perforation of the membrane using the antibiotic also takes a significant amount of time, and the duration is longest when using gramicidin.

3.9. Kinase regulatory sites phosphorylation on CCCs

The *SLC12* family is regulated by phosphorylation and dephosphorylation of specific serine/threonine residues. These residues are located differently between the Na^+-driven and K^+-driven families [134]. For the Na^+-driven family, these residues are located in the amino-terminal domain, a region conserved amongst NKCC1, NKCC2, and NCC [181,182]. In contrast, the phosphorylation sites of the K^+-driven family are located in the carboxy-terminal domain.

Serine-threonine phosphorylation activates the Na^+-driven family, resulting in Na^+ influx and inhibits the K^+-driven family, which causes a decrease in K^+ efflux. Conversely, dephosphorylation of serine-threonine residues leads to the deactivation of the Na^+-driven family, while activation of the K^+ driven family occurs [111]. This results in the inhibition of Na^+ influx and an increase in K^+ efflux, respectively. Therefore, phosphorylation of the *SLC12* transporters appears to be a representation of the cotransporter activity.

Researchers often utilize large-scale phospho-proteomic profiling to identify phosphorylation sites. This approach involves identifying phospho-peptides and sequencing the phosphorylated residues through mass spectrometry (MS) [183]. The highly sensitive and specific nature of MS has led to its coupling with chromatographic techniques such as liquid chromatography (LC), resulting in a robust analytical technique known as LC-MS [184]. Two commonly used strategies for LC-MS/MS analysis of phosphorylation differ in their sample preparation. One approach involves identifying phosphorylation sites from individual proteins and small protein complexes, while the other involves identifying global phosphorylation sites from whole cells and tissue extracts. The first approach, as shown in Fig. S2 and detailed in Section S6 in the Supplementary data [72,134], involves the immunopurification of labeled proteins from cell lysates, followed by their purification via sodium dodecyl sulfate (SDS)-polyacrylamide gel electrophoresis (PAGE). The band of interest is excised from the gel and enzymatically digested into peptides before analysis by LC-MS/MS. For the latter method, the whole cell lysate is first digested and then peptide fractionation is done using strong cation exchange chromatography. After that, the samples are enriched for phospho-peptides using immobilized metal affinity chromatography (IMAC) or titanium dioxide (TiO_2) before conducting LC-MS/MS analysis. Another approach could be to fractionate the protein lysate using SDS-PAGE, followed by digestion, and enrichment of phospho-peptides by IMAC or TiO_2 before conducting LC-MS/MS analysis [185]. While global phosphorylation analysis has revealed numerous phosphorylation sites in various tissues, the process is
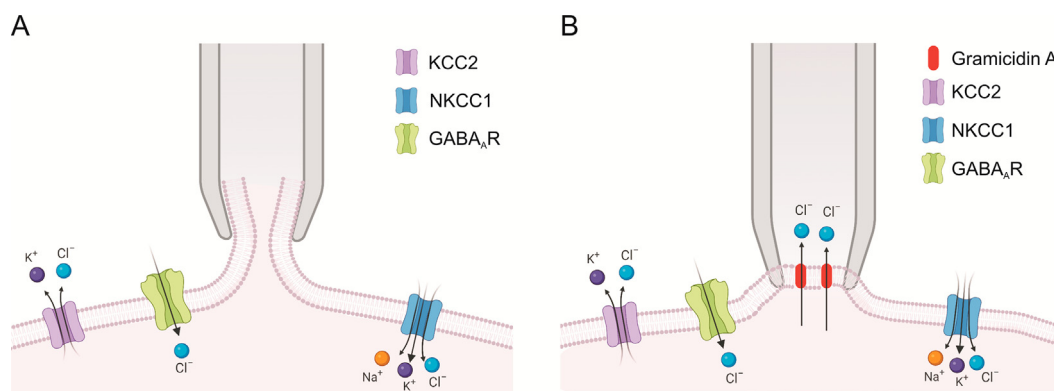
Fig. 5. Schematic depiction of the gramicidin-perforated patch clamp configuration and the whole-cell recording configuration. (A) Whole-cell recording involves recoding currents through multiple channels simultaneously. (B) The perforated patch technique uses antibiotic agents such as gramicidin to create cation-selective pores in the membrane. The diagram was created using BioRender.com. KCC2: K^+-Cl^- cotransporter 2; NKCC1: Na^+-K^+-Cl^- cotransporter 1; GABA: γ-aminobutyric acid; $GABA_AR$: $GABA_A$ receptor.

time-consuming and requires a significant amount of material. Both strategies have been used to identify phosphorylation sites for some *SLC12* family CCC members [186] and confirm the phosphorylation of sites for mKCC2 [170].

After the samples are prepared, the peptides of interest are introduced into a stationary phase (LC column) by a mobile phase flowing at high pressure. After chromatographic separation, the effluent is directly introduced into the mass spectrometer. The molecules are ionized using an ionization source and then migrate through a set of mass analyzers acting as magnets, which further separate molecules based on their mass-to-charge ratio. The peptides are sequenced by colliding with charged particles, causing fragmentation at the amide bonds along the backbone. This process occurs in the presence of an inert gas, and the resulting fragments are detected using an electron multiplier. Peptide sequences and their phosphorylated counterparts can be identified using informatics software after the sequencing step. The cascade of processes involved in the ion transition is highly specific to the structure of the molecule of interest, resulting in a high degree of selectivity [187]. LC-MS/MS has been utilized in various studies to identify and analyze phosphorylation sites on CCCs and their regulatory proteins, as summarized in Table S2 [72,134,182,186,188–194]. Furthermore, LC-MS/MS has been utilized in various studies to analyze and identify sites of phosphorylation on CCCs and their regulatory proteins, as well as to identify domains of regulatory proteins, enhancing our understanding of regulatory networks such as the WNK-SPAK/OSR1-CCC pathway [134,193,195–197].

Phosphorylation alterations in the *SLC12* family can be identified by employing phospho-specific antibodies that target phosphopeptides through a technique called western blotting. Western blotting is a procedure employed to detect a particular protein of interest within a sample of cells or tissue. In this approach, proteins are initially separated based on their size through electrophoresis. Subsequently, the separated proteins are transferred electrophoretically onto a solid support, typically a polyvinylidene difluoride or nitrocellulose membrane. A particular protein of interest is then identified through specific antibody marking. These antibodies are usually conjugated with tags or fluorophores that can be detected using different colorimetric, chemiluminescent, or fluorescent methods. This permits the detection of a specific protein of interest from a mixture of proteins. This method has been utilized to characterize the phosphospecific sites of KCCs [134] and has been used to discover inhibitors of KCC3 that can act against KCC3 Thr991/Thr1048 phosphorylation [198].

Phosphorylation alterations can also be quantified through immunoprecipitation, a technique that involves isolating a specific protein from a solution using antibodies and agarose beads [199]. Immunoprecipitation can be employed to isolate phosphorylated proteins with specific residues. Antibodies specific to the phosphorylation site, bound to protein G-sepharose, are used for this purpose. After separation from the protein mixture, the protein of interest is isolated by electrophoresis as described previously. It has been found, using immunoprecipitation, that KCC2 modulates cotransporter activity through phosphorylation at the KCC2 Thr906 and Thr1007 sites [175], and molecules that decrease KCC2 Thr1007 phosphorylation have been identified [200]. For a comprehensive overview of the recently characterized key KCC2 phosphorylation sites, please refer to Fig. S3.

It should be noted that the Western blotting technique can only provide semi-quantitative data since it offers a comparison of protein levels relative to one another rather than an absolute measurement of quantity. Differences in loading and transfer rates between samples in different lanes could vary across separate blots, which can result in inconsistencies. The signal generated by the Western blot technique is not linear and does not accurately reflect the concentration range of the samples being analyzed [201]. It is worth mentioning that protein activity cannot be solely inferred from its phosphorylation status since various factors such as inhibitors, mutations, and protein interactions with its surroundings could directly impact the protein's activity, independent of its phosphorylation level [202–204]. This observation is evident in the study by Hannemann and Flatman [205] in 2011, where the phosphorylation of the amino terminal of both NKCCs and their transport activity was compared using phospho-specific antibodies and $^{86}Rb^+$ in HEK293 cells stably expressing NKCC1 or NKCC2. Although the researchers observed reduced phosphorylation and transport during kinase inhibition, increased phosphorylation resulted in transport stimulation but not increased transport. This finding implies that while the phosphorylation of the amino terminal of the NKCCs may indicate the transporter's capability to move ions, the transport activity is influenced by other factors as well. Therefore, phospho-specific antibodies cannot provide an accurate measure of transport activity. For NKCC1, these extenuating factors, which include interactions with cytoskeletal proteins, influence its transport rate independently of phosphorylation [202,203]. Therefore, while phospho-specific antibodies can offer insights into cotransporter phosphorylation and the associated signaling pathway, relying solely on them for predicting cotransporter activity may not be correct. Instead, it may be more advantageous to utilize an alternate approach and consider phospho-specific antibodies as a supplementary tool. However, given that the expression of NKCC2 is highly restricted and the protein is difficult to express

in mammalian cell cultures, studies using phospho-specific anti-bodies may be less demanding than transport studies for studying its role in the kidney [206].

For Western blot analysis of KCC2, multiple oligomerization studies [175,207] have reported a multi-band migration pattern across the gel, instead of a single band. The lower band (~135 kDa) on the gel represents the monomeric form of the transporter, while the upper band (~270 kDa) represents oligomers or complexes of high molecular weight proteins that show resistance to denaturing conditions. Interestingly, the formation of KCC2 oligomers depends on the experimental procedure, particularly when KCC2 is over-expressed in heterologous systems or when samples undergo prolonged extraction (more than 4 min). These aggregates have been observed to be resistant to SDS, which is commonly used to denature proteins through heating or under acidic conditions [208]. The presence of KCC2 oligomers in biochemical analyses could pose a challenge as they may not accurately reflect the presence of functional dimers in the original tissue, leading to false negatives and positives [208]. However, in the aforementioned studies on KCC2, the overall signal intensity, which includes both the monomer and the aggregates, is used for quantitative analysis of the total protein expression [175,209]. A comprehensive proto-col has been recently described for investigating KCC2 functions and activities using Western blotting with phospho-specific anti-bodies [210].

3.10. Cl$^-$ sensitive microelectrodes

One of the earliest methods for measuring intracellular Cl$^-$ levels involved the use of chloride-sensitive microelectrodes. This technique employs a glass micropipette with a hydrophobic ion-selective membrane at the tip. An ion-dependent electric poten-tial is then measured across this membrane. An aqueous salt so-lution fills the rest of the pipette behind this membrane and offers a low-resistance pathway to the half-cell. The half-cell, typically an AgCl electrode, can either be a fine AgCl wire that protrudes from the end of a capillary glass or silver chloride located inside the tip of a micropipette. The ion-selectivity of the membrane plug gives an output voltage dependent upon the activity of the ion bathing the tip [211]. This technique was used in several studies in the giant axons of squid [212] and the crayfish [213] before it was demon-strated that not all AgCl microelectrodes are suitable for intracel-lular chloride measurements as the electrodes developed errors in the intracellular environment and produced inaccurate measure-ments with high values [214]. The general steps are summarized in Section S7 in the Supplementary data [212–214]. The ion-sensitive surface of the electrode must be completely contained within the cell, which poses a limitation on its applicability to small cells because of its relatively large size. Despite the tip diameter being less than one micron, the sensitive area spans ten microns in length and has a diameter of five microns [215]. The electrodes have un-dergone enhancements, including the development of a new electrode that employs a liquid ion exchanger membrane as its sensitive component. This membrane is created by placing a liquid ion exchanger within a holder in such a way that one side of the membrane is in contact with an aqueous reference solution, while the other side is in contact with the solutions to be analyzed. These modifications have been introduced by researchers recently. This refers to the siliconized borosilicate glass micropipette. The tip of the electrode is filled with a small amount (1–2 μM) of liquid chloride ion exchanger, allowing for a rapid response to changes in Cl$^-$ within 1–2 min. However, preparing these electrodes is a tedious process, and preventing damage during cell penetration can be challenging. Although the use of double-barrel pipettes can

prevent such damage when working with a single cell [216], it is necessary to use larger cells to obtain accurate recordings without causing damage. Cell penetration may also result in alterations to the original distribution of intracellular Cl$^-$. This method is tedious and cannot be used for high-throughput screening (HTS) applica-tions. Other disadvantages include size and potential effects on cell integrity are discussed in Section S8 in the Supplementary data.

3.11. Radiotracer ^{36}C$^-$

To investigate the intracellular chloride concentration, one method is to utilize a tracer uptake assay using ^{36}Cl$^-$ to characterize Cl$^-$ conductance, involving measuring the intracellular accumula-tion of radioactive chloride. This approach starts by incubating cultured cells in a medium containing ^{36}Cl$^-$ and labeling the cells with the radiotracer (step 1: labeling cells with ^{36}Cl$^-$). The length of the incubation time required for the radiotracer to diffuse into the cell can vary between 30 and 120 min. Following the loading phase, the cells are washed rigorously with a substantial quantity of an efflux buffer that is free of the radiotracer, to eliminate extracellular radioactivity (step 2: washing labeled cells). The washing process is critical since high levels of extracellular radioactivity can poten-tially obscure any radioactivity efflux from the cells. The residual radioactivity is extracted (step 3: extracting labeled cells) and measured using a liquid scintillation counter (step 4: measuring radioactivity) [217]. To calculate the intracellular chloride concen-tration, the amount of labeled chloride in the extracted sample is divided by the total amount of water present in the intracellular space of the sample (step 5: calculating intracellular chloride con-centration). One drawback of using the radiotracer ^{36}Cl$^-$ is due to its long half-life of 300,000 years, which could pose a safety hazard for HTS applications [218]. Despite this limitation, the method has been utilized to investigate ion fluxes of NKCCs [219].

3.12. Fluorescent dyes

Advancements in cell biology and microscopy have led to the adoption of non-invasive fluorescent probes sensitive to Cl$^-$ for measuring intracellular chloride concentrations. One early appli-cation of fluorescent dyes involved the utilization of the quench-ing property of halides on the fluorescence intensity of heterocyclic organic compounds with quaternary nitrogen. Elevated levels intracellular chloride leads to a decrease in fluo-rescence intensity. MQAE is the most commonly used organic dye for this purpose. MQAE is excited at ultraviolet wavelengths of 350 nm, and its emission fluorescence is recorded at 460 nm. MQAE, unlike other Cl$^-$ indicators such as 6-methoxy-N-ethyl-quinolinium iodide or 6-methoxy-N-(3-sulphopropyl)quinoli-nium, has high water solubility and cell membrane permeability, which help reduce the incubation time required for using this dye. It is also not pH sensitive. Despite their high sensitivity and selectivity to chloride ions, these organic dyes are susceptible to bleaching since they are excited at ultraviolet wavelengths. This limits the time of measurements and make it challenging to ac-quire data at a low acquisition rate (0.1–2 frames per min). Other disadvantages include a significant leakage rate (3%–30% per h) and the inaccessibility of ratiometric measurements [216]. Recent advancements in microscopy have addressed the limitations of organic dyes by utilizing two-photon excitation in combination with a fluorescence-lifetime imaging microscopy [220]. This approach has successfully resolved issues such as bleaching and photochemical damages. Particularly, the use of red or infrared light minimizes the photo damage by ultraviolet light. This com-bination also allows for in vivo visualization of neurons and

astrocytes and monitoring of changes in intracellular chloride concentration in many individual cells. MQAE-based probes have been effectively utilized for precise measurement of Cl^- transport in glial cells [221]. They have also been developed into the first mitochondrial Cl^--sensitive fluorescence probe, Mito-MQAE [222], and have been applied to high-throughput screening of NKCC1 modulators, which led to the identification of a novel selective inhibitor of NKCC1 [223].

3.13. Genetically encoded sensors

An alternative approach is to use genetically encoded chloride sensors (GECS), which involves expressing chromophores such as yellow fluorescent protein (YFP) and green fluorescent protein (GFP) endogenously. YFP binds to halides and is sensitive to chloride. These sensors for chloride utilize fusion proteins composed of a halide-sensitive protein such as YFP or GFP and a halide-insensitive protein like C-reactive protein, red fluorescent protein from *Discosoma* sp., or tandem dimer Tomato, connected via a brief linker. The first variant of YFP, Clomeleon, enables ratiometric measurements and, thus, estimation of the level of $[Cl^-]_i$ at an half maximal effective concentration (EC_{50}) of 167 mM. The sensitivity of the Clomeleon sensor was gradually enhanced (EC_{50} 30–50 mM), and a more sensitive probe, called Cl^--sensor, was developed. Later, a transgenic mouse encoding both Clomeleon and Cl^--sensor was successfully generated. The Clomelon probe and its derived Cl^--sensor have been successfully applied to detect alterations in intracellular chloride levels resulting from the activity of KCC2 or NKCC1 in neurons [224,225]. More recently, YFP has been used to measure NCC activity [226]. Biosensors based on YFP enable excitation in the visible wavelength range and can be directed to specific cell types through plasmid transfection or transgenic animals carrying inserted genes.

These YFP-based biosensors have a large molecular weight that restricts the diffusion of indicators from the cell. However, they exhibit strong bleaching, which can be prevented by using two-photon microscopy, and are sensitive to some organic anions and intracellular pH. This can be problematic because the activities of $GABA_AR$ involve changes in both chloride ions and hydrogen ions' concentrations. Both Clomelon and Cl^--sensor have demonstrated sensitivity to these issues.

To measure intracellular chloride concentration more precisely, a GFP-based ratiometric biosensor called ClopHensor was developed. This sensor utilizes a mutated variant of GFP known as E2GFP, which is sensitive to both Cl^- ions and changes in pH, allowing for simultaneous monitoring of Cl^- and pH levels. More recent work involved the development of the neuronal variant, ClopHensorN, which is a derivative of ClopHensor designed for neuronal cell expression. While a previous study identified the formation of dense intracellular aggregations of the fluorescence protein component in ClopHensor, this issue has been addressed by substituting it with a more appropriate protein. In a recent investigation by Gagnon, a ratiometric fluorescent Cl^- sensor called Chlomelon was employed to detect substances that activate KCC2 in cells and decrease intracellular chloride levels. These cells were used as models for disease states involving GABAergic inhibitors, and the study successfully identified one KCC2-selective analog [227]. Furthermore, ClopHensor was also recently utilized [228].

Overall, GECS are advantageous for HTS applications as they allow for recording multiple cells and non-invasively measuring intracellular chloride concentrations in neuronal compartments, such as axons, dendritic spines, and shafts [218]. The GECS encoding cell lines can also be easily propagated, enabling the screening extensive collections of chemical compounds. However, the YFP-based chloride sensors utilized in these cell lines are susceptible to small anions that can modify the ionization constant of the chromophore and subsequently affect fluorescence emission, which is a potential drawback. Inaccuracies in measuring intracellular chloride concentrations, especially at basal levels, have been recorded to reach 10 mM at physiologically low intracellular chloride concentrations. In situations where there is a substantial variation in pH levels caused by neuron activity, genetically encoded pH sensors are essential to mitigate the impact of pH sensitivity. ClopHensor and its various derivatives can be utilized to achieve this goal. However, the new sensors require three excitation wavelengths for acquisition, compared to the two required by the previous generation of sensors. It is also advisable to utilize laser light sources since the two excitation wavelengths for ClopHensor are closely spaced. Additionally, the new sensors require an extra photodiode to measure laser power fluctuations during acquisition, which is crucial for correcting fluorescence ratios. Furthermore, the resulting dataset requires sophisticated analysis [218].

4. CCCs drug discovery

The physiological importance of *SLC12* family members has been confirmed by its association with human Mendelian diseases, as mentioned in Section 2.1. For a long time, the pharmacological profile of electroneutral CCCs, which are encoded by the *SLC12* family members, has been mainly influenced by a handful of drugs that specifically target cotransporters in the kidney, for example, the diuretics furosemide since the 1960s [229], and bumetanide since 1970s [230]. Over the past few years, increasingly apparent that the *SLC12* family members play a significant role in ion fluxes across a range of tissues. NCC is located on the luminal side of the epithelial cells in kidney's DCT, while NKCC2 is situated on the apical side of the epithelial cells in the TAL. These specific regions are responsible for the reuptake of salts and obligatory water from urine formation, which are crucial in maintaining electrolyte balance and regulating blood volume and pressure (Fig. 6A). In immature neurons, Cl^- currents mediated by $GABA_ARs$ are depolarizing and outward, attributed to a higher proportion of NKCC1 to KCC2 activity or an increase in NKCC1 and KCC2 phosphorylation through WNK-SPAK-dependent mechanisms. Healthy mature neurons maintain a low intracellular concentration of $[Cl^-]_i$ through the inverse activity pattern of NKCC1 and KCC2. This promotes hyperpolarization mediated by $GABA_AR$, crucial for maintaining the appropriate balance of excitation and inhibition in neuronal circuits (Fig. 6B). This has led to increasing interest in the discovery of novel small molecules that target the CCCs. Interestingly, as the family members of the *SLC12* cotransporters share a degree of homology, multiple drugs can influence family members. For instance, bumetanide and furosemide can block the activity of both NKCC1 and NKCC2 and may also affect the activity of KCCs. Various small molecules along with their respective target CCCs are summarized in Table 2 [223,231–243].

4.1. Medicinal chemistry effects for CCCs compounds, and their contribution in CCC biology

4.1.1. Thiazide

Systemic hypertension is a prevalent condition that, when left untreated, elevates the risk of renal failure, strokes, and coronary thrombosis. Before 1950, there was no efficient treatment available, making the development of antihypertensive medications a significant success story [244]. Indeed, thiazide diuretics were discovered in the 1950s when Merck Sharpe and Dohme's chemists

and physiologists tested sulfonamide-based carbonic anhydrase inhibitor derivatives, which aimed to enhance sodium and chloride excretion instead of sodium bicarbonate [244]. Hydrochlorothiazide was the first thiazide diuretic to receive U.S. FDA approval in 1959 and is the most commonly prescribed drug to treat edema and hypertension [245,246], and, recently, in chronic kidney disease [247]. Investigators have long been puzzled by the mechanisms through which these drugs efficiently reduce arterial pressure [248]. Thiazides cause an acute reduction in cardiac output by decreasing extracellular fluid (ECF) and plasma volume. However, with chronic use, ECF volume tends to return to its original level, and vasodilation takes over [249]. Some earlier studies suggested that the main mechanism through which thiazide diuretics decrease arterial pressure is direct vasodilatation, which could be facilitated by changes in how ions are transported within the blood vessels [249]. Despite this, the primary function of thiazide diuretics is to directly block NCC in the DCT of the kidney [250]. Thiazide diuretics are specific inhibitors of NCC, as they do not inhibit the furosemide-sensitive NKCC [251]. Fan et al. [9] recently used cryo-electron microscopy (Cryo-EM) to identify the human NCC structures, which formed a complex with a co-crystallized thiazide diuretic. This discovery demonstrates the specific interaction between thiazide diuretics and NCC and how they obstruct the transport of ions. By overlapping with the suggested Cl^- binding site on NCC, the chloro group situated in the six-position of polythiazide presents significant proof that thiazide diuretics compete with Cl^- for binding [9]. This observation supports the notion that thiazide diuretics and Cl^- compete for the same binding site.

4.1.2. Bumetanide

Bumetanide is a diuretic drug approved by U.S. FDA and widely used due to its high potency. It displays a 500-fold greater affinity for NKCCs than KCCs [252]. The discovery of bumetanide dates back to 1969 during studies on a vast group of diuretic derivatives of 3-amino-5-sulfamoylbenzoic acid, and the chemical structures and biological activities of these derivatives underwent systematic analysis [253]. This discovery led to the synthesis of several related compound series with similar chemical structures and diuretic profiles [254,255]. In both humans and animals, bumetanide was discovered to be more potent than the loop diuretics furosemide and ethacrynic acid, which have been established as clinical treatments [256]. In 1979, Frizzell et al. [257] suggested that the diuretic effects of loop diuretics occur by blocking the activity of NCC in the kidney. Following this, Palfrey et al. [258] conducted a study in 1980 to examine the effects of various aminobenzoic acid derivatives, including some of the derivatives of bumetanide, on a system that transports cations together in avian red blood cells. This co-transport system was later identified as NKCC1 [259]. Together with the study by Lykke et al. [260] in 2015 on several bumetanide derivatives, a strong correlation exists between the effectiveness of diuretics in animal assays and their inhibitory potency in the avian cotransporter.

Following a brain injury, an accumulation of chloride in neurons leads to a favorable change in the reversal potential of chloride currents gated by GABA, which weakens the inhibitory effects of GABA neurotransmitters [224]. However, inhibiting the activity of NKCC1 after the injury reduces the accumulation of neuronal chloride [261]. As a result, GABA reversal potential aligns better with physiological values. This, in turn, enhances the effectiveness of anticonvulsants like phenobarbital that augment the average duration of GABA$_A$ channels in treating neonatal seizures [262]. An early pilot study in 2010 showed that bumetanide can reduce autistic behavior in five infants who received treatment for three months without any adverse effects [263]. A subsequent double-blind clinical trial was performed and found that bumetanide reduces intracellular chloride, reinforcing GABAergic inhibition [264]. A phase II randomized controlled trial conducted recently utilized bumetanide as a supplementary therapy for neonatal seizures and yielded a compelling indication of its efficacy while exhibiting no signs of toxicity signs [265]. However, the efficacy of bumetanide was investigated in another independent phase II superiority trial, which revealed unfavorable outcomes indicating that it did not have a superior impact on the primary outcome [266]. This may be due to bumetanide's physicochemical properties, exhibiting poor transport through the blood-brain barrier (BBB). In 2014, two ester
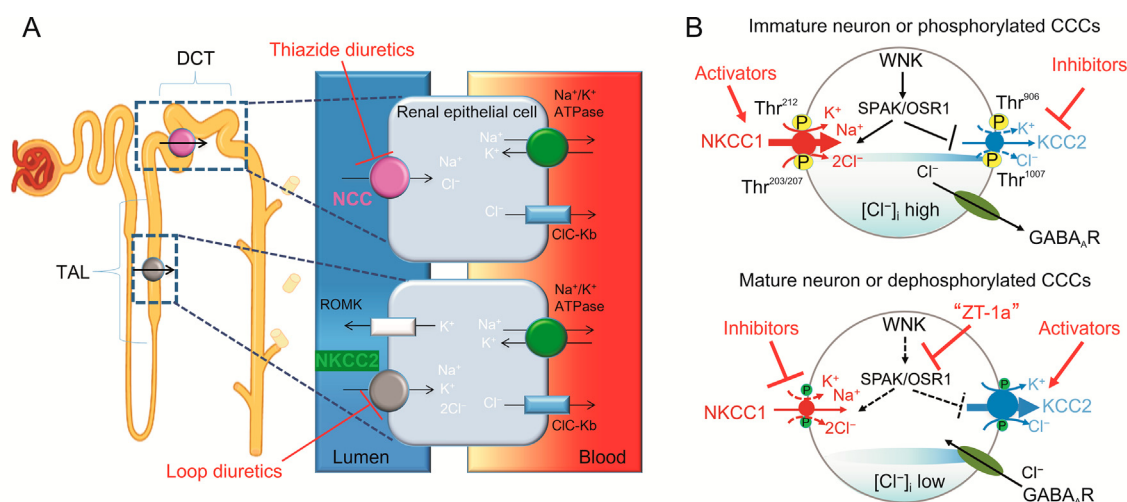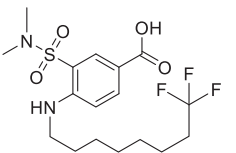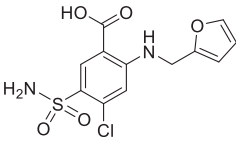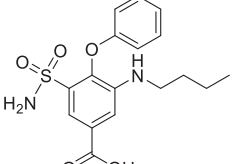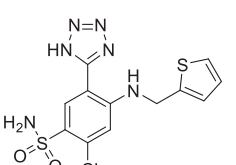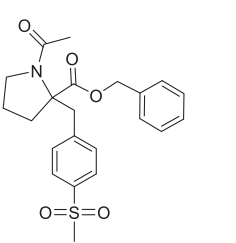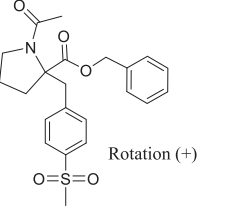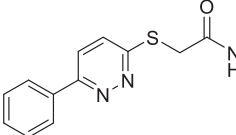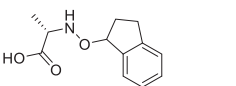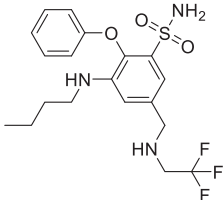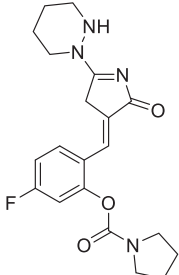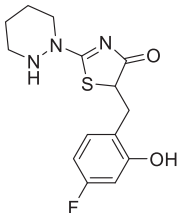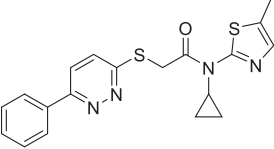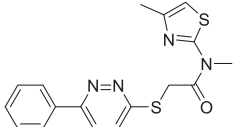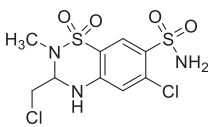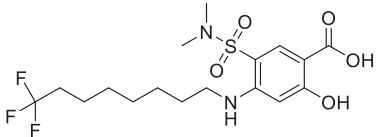

Fig. 6. The mechanism by which diuretic drugs target cation-chloride cotransporters (CCCs) in the kidney and how these transporters regulate Cl^- volume and the polarity of γ-aminobutyric acid (GABA) response in the nervous system. (A) Thiazide and loop diuretics inhibit Na$^+$-Cl$^-$ cotransporter (NCC) and Na$^+$-K$^+$-2Cl$^-$ cotransporter 2 (NKCC2), respectively, reducing salt and water retention in the kidney. (B) In immature neurons (upper panel), higher NKCC1 to K$^+$-Cl$^-$ cotransporter 2 (KCC2) ratio leads to outward and depolarizing Cl^- currents mediated by GABA$_A$ receptors (GABA$_A$Rs). In mature neurons (lower panel), the opposite activity pattern of NKCC1 and KCC2 maintains low intracellular chloride ion concentration ($[Cl^-]_i$), enabling GABA$_A$R-mediated hyperpolarization crucial for balancing neuronal excitation and inhibition. DCT: distal convoluted tubule; TAL: thick ascending limb; ROMK: renal outer medullary K$^+$ channel; ClC-Kb: Cl^- channel Kb; WNK: with-no-lysine (K) kinase; SPAK/OSR1: SPS/Ste20-related proline-alanine-rich kinase/oxidative stress-responsive kinase 1.

Table 2
Small molecules specifically target cation-chloride cotransporters (CCCs).

Compound	Chemical structure	Function	Binding target and IC_{50}	Refs.
ARN23746		Selective NKCC1 inhibitor	NKCC1 IC_{50} = 20 μM NKCC1 IC_{50} = 11.1 μM (in neurons)	[223,233]
Furosemide		NKCC inhibitor	NKCC1 IC_{50} = 10–50 μM NKCC2 IC_{50} = 15–60 μM KCC2 IC_{50} = 10 μM KCC3 IC_{50} = 25 μM KCC4 IC_{50} = 900 μM	[231]
Bumetanide		NKCC1 inhibitor	NKCC1 IC_{50} = 0.05–0.6 μM NKCC2 IC_{50} = 0.1–0.5 μM KCC1 IC_{50} = 60 μM KCC2 IC_{50} = 55 μM KCC3 IC_{50} = 40 μM KCC4 IC_{50} = 900 μM	[231]
Azosemide		NKCC1 inhibitor	NKCC1 IC_{50} = 0.246 μM	[232]
KCC2 blocker 1		Selective KCC2 blocker	KCC2 IC_{50} = 1 μM	[234]
(+)-KCC2 blocker 1	Rotation (+)	Selective KCC2 blocker	KCC2 IC_{50} = 0.4 μM	[234]
VU0240551		Selective KCC2 blocker	KCC2 IC_{50} = 0.560 μM	[235]
DIOA		Selective KCCs blocker	KCCs IC_{50} = 10 μM	[236]
OV350	Nto available by the time	Selective KCC2 activator	KCC2 EC_{50} = 0.261 μM	[237]

Table 2 (*continued*)

Compound	Chemical structure	Function	Binding target and IC$_{50}$	Refs.
STS66		NKCC1 inhibitor	NKCC1 IC$_{50}$ = 40 μM	[238]
CLP290		KCC2 activator		[239]
CLP257		KCC2 activator	KCC2 EC$_{50}$ = 0.616 μM	[239,240]
VU0463271		Selective KCC2 blocker	KCC2 IC$_{50}$ = 0.061 μM	[241]
ML077		KCC2 inhibitor	KCC2 IC$_{50}$ = 0.537 μM	[241]
Thiazide		NCC inhibitor	NCC IC$_{50}$ = 0.5 μM NKCC1 IC$_{50}$ = 31 μM	[242]
ARN24092		Selective NKCC1 inhibitor	NKCC1 IC$_{50}$ = 20 μM	[243]

IC$_{50}$: half maximal inhibitory concentration; NKCC: Na$^+$-K$^+$-2Cl$^-$ cotransporter; KCC: K$^+$-Cl$^-$ cotransporter; EC$_{50}$: half maximal effective concentration; NCC: Na$^+$-Cl$^-$ cotransporter.

prodrugs of bumetanide, i.e., pivaloyloxymethyl (or BUM1) and *N,N*-dimethylaminoethylester (or BUM5), were synthesized, and they were shown to produce substantially higher concentrations of bumetanide in the brain than administering the original drug [267]. In 2018, bumepamine, a benzylamine derivative of bumetanide that is lipophilic and has the ability to penetrate the BBB without hindering NKCC1, was discovered. It was observed to be more efficient

than bumetanide in augmenting phenobarbital's anticonvulsant properties in animal models [268]. STS66 is a new inhibitor of NKCC1 composed of 3-(butylamino)-2-phenoxy-5-[(2,2,2-trifluoroethylamino)methyl]benzenesulfonamide which has been found to be superior to bumetanide in terms of brain penetration and in reducing brain damage following ischemic stroke in mice [269]. In 2020, Savardi et al. [223] designed, synthesized, and

assessed new molecules in vitro to improve upon the existing compounds derived from bumetanide and other inhibitors of NKCC1. As a result, they developed a potent lead NKCC1 selective inhibitor, ARN23746, which showed no inhibition of NKCC2 and KCC2. In vitro studies showed that ARN23746 could modify neuronal chloride homeostasis, and animal experiments using Down syndrome (DS) and autism mouse models revealed that it could alleviate core symptoms [223]. Moreover, ARN23746 underwent extensive in vitro and in vivo preclinical evaluations, which served as a crucial step forward in the progress toward further clinical investigations [233]. The results indicated that ARN23746 exhibited a favorable profile regarding its potency, brain penetration, and metabolism. Additionally, the drug was found to be orally bioavailable, and it effectively improved cognitive impairments in mice of DS after oral administration, with no observed diuretic effects or toxicity [233]. Azosemide and torasemide are two loop diuretics that potently suppress the activity of NKCC1. Unlike furosemide and bumetanide, they do not have a carboxylic group, which makes them more capable of passively diffusing through biomembranes [270]. In a rat model of birth asphyxia, torasemide enhances the disease-modifying and anti-seizure effects of midazolam, whereas azosemide does not [270].

4.1.3. Furosemide

Furosemide was developed in the 1960s when scientists were searching for new treatments for congestive heart failure and hypertension. The production of furosemide involves a multistep synthesis process that utilizes 4,6-dichlorobenzoic acid-3-sulfonylchloride as a starting material. Ammonia and 6-furfurylamine are subsequently added to the reaction mixture sequentially [271]. Furosemide is a potent diuretic with a rapid onset of action. However, compared to bumetanide, furosemide exhibits non-selective inhibition of NKCCs and blocks KCC2 at similar concentrations [229]. Its applications extend from managing hypertension to treating edema caused by cardiac, hepatic, or renal issues, and even to providing symptom relief for hypercalcemia. In 1964, clinical trials of furosemide began, and the drug was found to be highly effective in treating edema and reducing blood pressure in patients who with congestive heart failure. Furosemide was approved by U.S. FDA in 1982 and has been included in the List of Essential Medicines by the World Health Organization. In addition to its effect on NKCCs, furosemide was found to inhibit KCC3 when it was cloned in 1999 [58]. Furosemide was also observed to have an inhibitory effect on KCC2. When 2 mM furosemide was applied, K^+ uptake in KCC2-expressing cells was completely blocked [272]. While furosemide inhibits the NKCCs at concentrations in the low micromolar range [252], it only affects the KCCs at significantly higher concentrations of approximately 100 μM or above [273]. High-affinity extrasynaptic $GABA_AR$s that contain the α4 and α6 subunits can be strongly inhibited by furosemide, but not bumetanide [274]. Furosemide has then been used to inhibit potassium-chloride cotransport by KCC2 to prevent sound-triggered seizures in rats prone to audiogenic seizures following an ischemic event [275]. Our recent study found that furosemide can restore GABA inhibition mediated by KCC2 and halt the progression from acute seizure to epileptogenesis by preventing the downregulation of membrane KCC2 during the induction of acute seizures [276].

4.1.4. Selective KCC2 activator

For a long time, the development of potent and selective activators for KCC2 has been a highly desired objective. In 2013, Gagnon et al. [227] discovered CLP257 (200 nM), which selectively increases KCC2 activity [227]. However, in 2017, Cardarelli et al. [176] were unable to replicate these results and proposed that CLP257 may exert its effects via potentiating $GABA_A$ receptors instead. Recently, Jarvi et al. [237] developed a KCC2-specific compound termed OV350 (or 350), which showed an EC_{50} of 261.4 nM for KCC2 and did not affect the function of NKCC1, KCC3, or KCC4. Additionally, it did not alter its plasma membrane accumulation or phosphorylation, both of which have been proposed as crucial factors for KCC2 function [175,277]. Subcutaneous administration of OV350 in mice exhibits significant brain penetration and CNS activity and does not induce any overt phenotype. KCC2 activation by OV350 protects against seizures caused by convulsant pentylenetetrazole, a $GABA_AR$ antagonist, and refractory seizures triggered by benzodiazepines, the canonical $GABA_AR$-positive allosteric modulators [237]. Therefore, OV350 is the first compound known to directly bind to and activate the KCC2 cotransporter, which shows promising potential for treating epilepsy.

4.1.5. Others

[(dihydroindenyl)oxy]alkanoic acid (DIOA) is much more specific for blocking KCCs rather than NKCCs. At a concentration of 100 μM, DIOA inhibits KCCs (half maximal inhibitory concentration (IC_{50}) of 10 μM), but it does not block NKCCs [18,236]. The characteristics of K^+ efflux sensitive to DIOA provide conclusive evidence that there exists a mechanism for the cotransportation of K^+ and Cl^- in human red blood cells, which plays a role in regulating cell swelling [236]. The K^+ transport experiments that complemented the study found that 50 μm DIOA completely eliminated both lipopolysaccharide- and phorbol 12-myristate 13-acetate-induced K^+ efflux, which was insensitive to ouabain and bumetanide. Despite its effects on K^+ efflux sensitive to DIOA in human red blood cells, this compound did not alter the basal Cl^- and K^+ efflux or affect the viability of resting human neutrophils [278]. Recently, we and others have also developed specific kinase inhibitors that target the upstream regulators of CCCs, the WNK-SPAK signaling pathway. For example, in 2016, Yamada et al. [110] made a breakthrough by identifying WNK463, a pan-WNK kinase inhibitor that can be taken orally. It has a high level of selectivity for kinases and an affinity in the low nanomolar range. When given orally, WNK463 was observed to considerably reduce blood pressure in a rat model of hypertension [110]. The development of WNK463 as a potential treatment was halted due to the discovery of additional effects beyond those observed in the renal and cardiovascular systems when administered at higher concentrations to rats [279]. Nevertheless, a study conducted by Lee et al. [177] in 2021 showed that WNK463 can be effective in reducing the occurrence and frequency of seizure-like events in a slice model of seizures induced by 4-aminopyridine. The drug achieved this by enhancing KCC2-mediated Cl^- export and causing hyperpolarization of E_{GABA} [177]. A specific inhibitor for SPAK, ZT-1a (5-chloro-N-(5-chloro-4-((4-chlorophenyl)(cyano)methyl)-2-methylphenyl)-2-hydroxybenzamide), has recently been developed [138]. It functions as a modulator for both KCCs and NKCC1 by promoting KCCs and inhibiting NKCC1 through a decrease in their phosphorylation that is dependent on SPAK [138]. Inhibiting SPAK leads to an improvement in the export of K^+ that is dependent on Cl^- and allows for better cellular volume regulation after injury. Animal studies have shown that ZT-1a can lower the level of CCC phosphorylation caused by ischemia, which can reduce cerebral edema and lead to better results in terms of functionality [138]. Given its specificity and positive results in vivo, ZT-1a has the potential to be a highly effective treatment for cerebral edema.

5. Functional and structural investigation of CCCs by Cryo-EM technology

Cryo-EM of single particles is a method employed to investigate the configuration of large biological molecules, such as proteins, viruses, and ribosomes, at high resolution. The technique was first developed in the 1980s [280] and has undergone significant technological advancements in recent years [281]. It received the Nobel Prize in Chemistry in 2017 due to its impact on structural biology and biomedicine [282]. The process of Cryo-EM entails rapidly freezing a biological macromolecule sample in a layer of vitrified ice, followed by imaging the particles with an electron microscope. Subsequently, the pictures are analyzed and combined to generate a precise three-dimensional (3D) model of the macromolecule through averaging. The workflow from purified protein samples to the 3D model is shown in Fig. S4. Cryo-EM has several advantages over traditional crystallography, including the ability to study large and flexible macromolecules that are difficult to crystallize and the ability to study macromolecules in a near-native, hydrated state. Furthermore, Cryo-EM allows for the study of macromolecules that exist in multiple conformations, as it provides an average representation of the entire population of macromolecules in the sample. Cryo-EM has revolutionized the field of structural biology and has enabled the determination of structures for many previously intractable biological systems. As a result, novel information regarding the roles and operations of biological macromolecules has emerged, opening up new opportunities for the creation of innovative medications and treatments.

Previously, conventional hydropathy analysis revealed that CCCs are identified by their transmembrane domain (TMD), which consists of 12 helices, as well as their extensive extracellular domains and substantial cytoplasmic N- and C-terminal domains [33,37]. Recently, high-resolution structures of almost all CCCs, except for NKCC2, including NKCC1 [7,8], NCC [9,10], KCC1 [11], KCC2 [12,13], KCC3 [12,13] and KCC4 [13,14], in various ionic environments where ion-binding sites may be partially or fully occupied, or completely vacant (Fig. 7A). The TMD is readily apparent in the structures of all CCCs, but for certain structures, the extensive C-terminal domain displays incomplete density, which could be attributed to its diverse orientations below the TMD [283,284]. The TMD of CCCs exhibits a conventional leucine transporter fold, with the substrate transport core consisting of two inverted repeats of TM1−5 and TM6−10. Meanwhile, the two remaining helices (TM11 and TM12) might play a role in the dimeric assembly [283−285]. Within the ion transport pathway, the TM1 and TM6 helices occupy a central position and interrupt the α-helical geometry at the midpoint of the lipid bilayer. The sites for ion binding are arranged surrounding these noncontinuous hinge regions [283−285]. The domains located at the C-terminus of NKCC1 [7,8], NCC [9,10], and KCCs [12−14] have a high degree of conservation and share an identical ten-stranded β sheet core. The structures of KCC2 [12,13], KCC3 [12,13], and KCC4 [13,14] reveal that an autoinhibitory segment at the N-terminus is inserted and acts as a physical barrier at the point where the ion permeation pathway opens into the cell's interior (Fig. 7A). This indicates that the cytoplasmic vestibule must be cleared of this segment when KCCs are actively transporting ions.

Further, CCCs structures have been determined in complex with diuretic drugs (Fig. 7B), such as human NKCC1 and bumetanide and furosemide [283], human NCC and thiazide diuretic [9], or with small molecule inhibitors, for example, human KCC3 and DIOA [12], and human KCC1 and VU0463271 [284]. These findings offer an initial atomic-level understanding of the interactions between these inhibitors and different CCC transporters and their effects on

ion transportation. Bumetanide binds to the ion translocation pathway on the extracellular side, which includes highly conserved residues in both human NKCC2 and NKCC1 [283]. This is the reason why bumetanide, as well as other loop diuretics, is unable to distinguish between these two highly similar paralogs. Therefore, future co-structure work on NKCC1 and ARN23746 would be interesting to explain why ARN23746 is an NKCC1 selective inhibitor.

6. Established HTS methods for specific CCCs compound

6.1. HTS screening for KCC2 modulator

Conventional techniques employed to evaluate the activity of CCCs are not suitable for HTS. In 2009, Delpire et al. [168] developed a fluorescence-based approach suitable for HTS to discover small molecules or compounds that impact KCC2 activity (Fig. 8A). Their method involves utilizing a fluorescent dye that reacts to Tl, a cation that is transported by CCCs (as mentioned in Section 3.7). The assay's strength was assessed by computing the Z', a statistical metric utilized for evaluating the robustness of an HTS assay [286]. They used this approach to screen a library of 234,560 compounds with an average Z' value of 0.686, across several 384-well plates growing with HEK293 cells overexpressing KCC2. They discovered 465 compounds that displayed a typical dose dependence in inhibiting KCC2 activity. After evaluating their strength and chemical structure, they chose 26 compounds that hindered the rise in Tl-induced fluorescence and conducted tests on their impact on the functions of NKCC1 and KCC2 through radioactive rubidium ($^{86}Rb^+$) uptake experiments on HEK293 cells. They then focused on a compound termed D4, *N*-(4-methylthiazol-2-yl)-2-(6-phenylpyridazin-3-ylthio)acetamide, which noticeably suppressed K^+ uptake mediated by KCC2 at 10 μM while exhibiting minimal impact on NKCC1. By employing a structure-activity relationship analysis, they designed a series of molecules based on the structure of D4. As a result, they produced two potent analogs, D4/6m (CID 25067404, or ML077) and D4/6l (CID 7211972), with EC_{50} values of 537 and 558 nM, respectively. Subsequently, they carried out additional chemical lead optimization of ML077, resulting in the development of a highly potent antagonist probe termed VU0463271 for KCC2 [241]. VU0463271 displays over 100-fold specificity towards NKCC1 and exhibits no activity against a wider range of ion transporter, ion channels, and G protein-coupled receptors (GPCRs). The application of VU0463271 both in vitro and in vivo has been shown to result in neuronal excitability [287,288]. Recording muscimol-induced currents from rat reticular thalamic (RT) neurons through in vitro gramicidin perforated patch technique, the administration of 10 μM VU0463271 led to a more depolarized E_{GABA} of RT neurons as compared to the baseline [287]. According to Sivakumaran et al. [288], the use of VU0463271 at a concentration of 10 μM caused a shift towards depolarization of E_{GABA}, changing it from -76 ± 5 mV to -36 ± 2 mV. The activity of KCC2 was abolished by 10 μM VU0463271, as evaluated by ex vivo electrophysiology, revealing that the spiking frequency of CA1 pyramidal neurons increased upon treatment [289].

In 2013, Gagnon et al. [227] conducted a screen to assess the activity of KCC2 by measuring the intracellular Cl^- concentration of neuroblastoma × glioma NG108-15 hybrid cells. To evaluate KCC2 function, cultured cells were transfected with Clomeleon, a chloride indicator. Following this setup, they started screening a collection of 92,500 compounds, leading to the identification of 78 positive hits. Subsequently, they performed a secondary screening to identify compounds that exhibited specificity towards cells
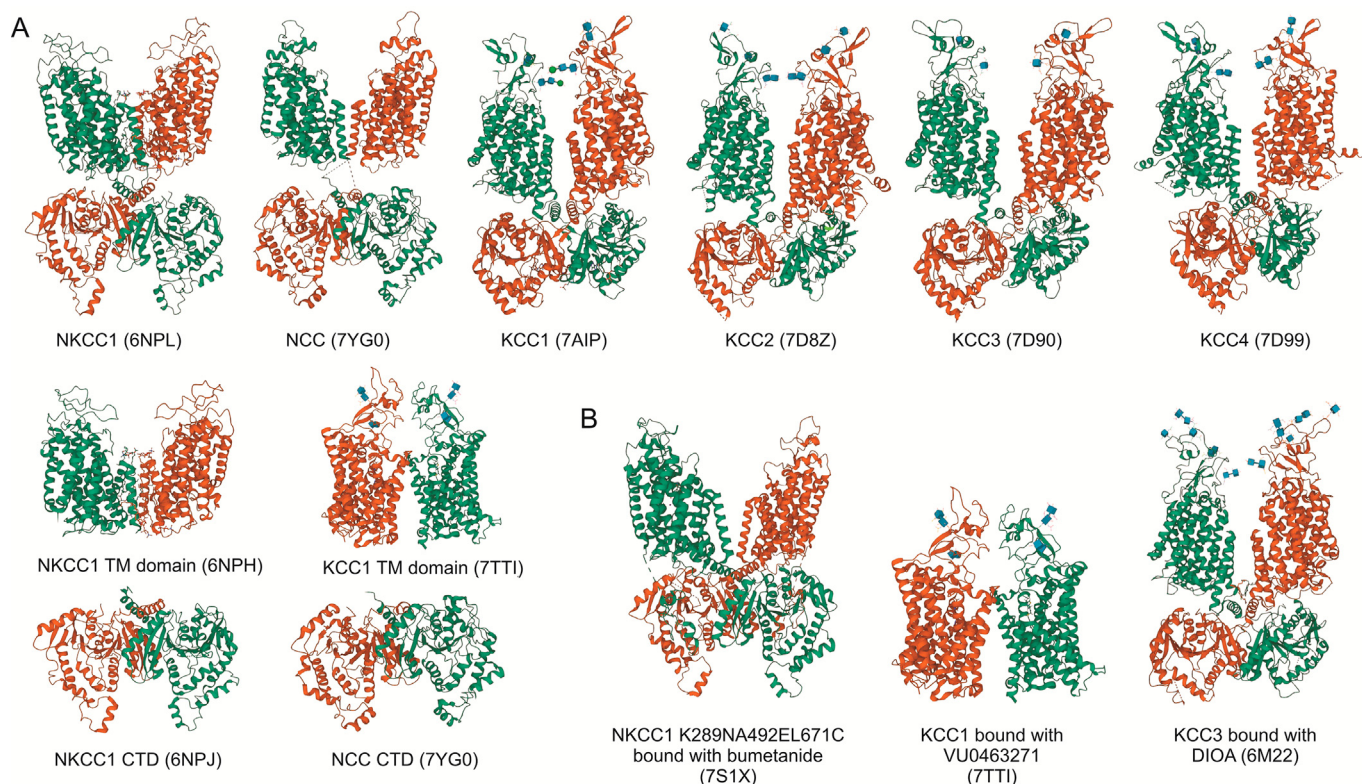
Fig. 7. Overall cryo-electron microscopy (Cryo-EM) structures of Na$^+$-K$^+$-2Cl$^-$ cotransporter 1 (NKCC1), Na$^+$-Cl$^-$ cotransporter (NCC), and Na$^+$-Cl$^-$ cotransporters (KCCs). (A) Cryo-EM structures of selected cation-chloride cotransporters (CCCs). From left to right: human species of NKCC1, NCC, KCC1, KCC2, KCC3, KCC4, NKCC1 TM domain, NKCC1, KCC1 TM domain, and NCC C-terminal domains (CTD). (B) CCCs structures in complex with diuretic drugs. From left to right: human NKCC1 K289NA492EL671C bound with bumetanide, KCC1 bound with VU0463271, and KCC3 bound with DIOA. Codes of cryo-EM structures that were submitted in the Protein Data Bank (PDB) are indicated below each image. Transmembrane domain (TMD) is colored in green, CTD in marine, and scissor helix in yellow. DIOA: [(dihydroindenyl)oxy]alkanoic acid.

expressing NKCC1, KCC1, KCC2, and KCC4, as well as towards a compound called CL-058, which contains three rings with a middle thiazol group, namely (5Z)-5-[(2-hydroxyphenyl)methylidene]-2-piperidin-1-yl-1,3-thiazol-4-one. Using CL-058 as a starting compound, they synthesized 300 analogs and discovered a lead compound termed CLP257. CLP257 was modified by adding an Fl$^-$ ion to the hydroxyphenyl group and replacing the pyridine group with a pyridazine. This resulted in a significant increase in potency, with an EC$_{50}$ decreasing from 31.5 mM to 50 nM. It is noteworthy that the specificity of CLP257 appeared to be limited to KCC2, as there was no indication of increased transport observed in a rubidium flux assay conducted on *Xenopus laevis* oocytes expressing other CCCs [227].

In order to discover compounds that enhance KCC2 function, in 2022, Prael Iii et al. [290] created a KCC2 activity assay compatible with HTS. The assay employs a monoclonal HEK293 cell line that expresses KCC2 in an inducible manner and constitutively expresses the Cl$^-$ sensor SuperClomeleon [291]. They utilized variations in the fluorescence of SuperClomeleon, which indicate changes in intracellular chloride concentration [Cl$^-$]$_i$, as a measure of KCC2 activity (as mentioned in Section 3.13). They screened ~23,000 small molecules, and the assay's strength was quantified using the Z' method [286]. The compound known as VU0500469 displayed a distinctive pharmacological profile as it enhanced the activity of KCC2 in neurons and prevented seizure-like events in vitro. In the future, efforts should be made to improve the effectiveness of compounds in the VU0500469 category. Additionally, a comprehensive evaluation will be conducted to determine the specificity of compounds similar to VU0500469 against a wide range of targets, along with gaining a more thorough understanding of how VU0500469-like compounds enhance the activity of KCC2.

Jarvis et al. [237] in 2023 employed a drug screening process involving multiple tiers to detect chemical compounds capable of directly activating KCC2. In this experiment, the researchers utilized HEK293 cells that overexpressed KCC2 to conduct Tl influx assays. They then tested the effect of 1.3 million compounds from AstraZeneca's compound library on potassium flux at a concentration of 30 μM. Afterward, they chose compounds for further analysis based on their capacity to enhance KCC2 activity, but not KCC3, KCC4, or NKCC1, by over 30% with an EC$_{50}$ of less than 30 μM. The researchers carried out an investigation to eliminate the possibility of compounds indirectly regulating KCC2 activity by altering its phosphorylation at Ser940 and Thr1007 sites. They accomplished this by analyzing the effects of the compounds on a set of 348 protein kinases. By eliminating compounds that exhibited kinase activities with an IC$_{50}$ value of less than 10 μM, the researchers identified a cluster of fused aminopyrimidine compounds, with compound 1 (Cmp1) serving as the representative molecule. Cmp1 displayed the ability to enhance KCC2 activity, with a lower EC$_{50}$ value of 2.01 μM. It is worth noting that this concentration had no effect on the activity of other solute carriers, such as KCC3, KCC4, or NKCC1, which are also involved in the neuronal Cl$^-$ homeostasis regulation. A cellular thermal shift assay was performed to confirm the direct interaction between Cmp1 and KCC2. To investigate the impact of Cmp1 on the thermal stability of KCC2, HEK293 cells were used to transiently express KCC2. The results showed that Cmp1 caused KCC2 to become unstable, with an IC$_{50}$ value of about
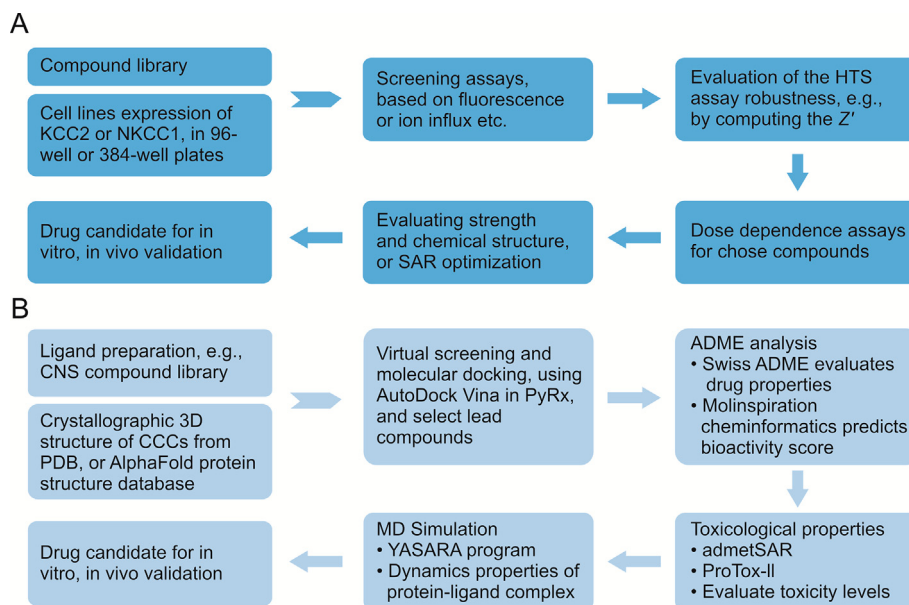
Fig. 8. General workflows of high-throughput screening of K^+-Cl^- cotransporter 2 (KCC2) or Na^+-K^+-$2Cl^-$ cotransporter 1 (NKCC1) modulators. (A) The overall workflow of high-throughput screening of KCC2 or NKCC1 compounds from compound libraries, followed by structure-activity relationship (SAR) optimization of drug candidates for in vitro and in vivo validations. (B) The overall workflow of high-throughput screening for NKCC1 inhibitors through in silico modeling, molecular docking, molecular dynamics (MD) simulation, evaluation on the absorption, distribution, metabolism, and excretion (ADME) properties, carcinogenicity, and toxicological and biological activities of the chosen compounds. HTS: high-throughput screening; CNS: central nervous system; 3D: three-dimensional; CCCs: cation-chloride cotransporters; PDB: Protein Data Bank; YASARA: Yet Another Scientific Artificial Reality Application.

1.1 µM. One of the derivatives generated, OV350 (or 350), showed an EC_{50} of 261.4 nM for KCC2 during the medicinal chemistry optimization process, which started with Cmp1 as the initial compound. OV350 can penetrate the brain and reduce the accumulation of neuronal chloride ions, thereby decreasing excitability. When activated, KCC2 by OV350 prevents the onset of status epilepticus induced by benzodiazepines, thereby reducing the risk of neuronal cell death [237], as discussed in the above section.

6.2. HTS screening for NKCC1 inhibitor

In 2017, Gill et al. [292] showcased the utilization of Aurora's Ion Channel Reader (ICR, ICR8000™/ICR12000™) as an alternative to traditional radioactive-based assays for studying NKCC1 and conducting high-throughput drug screening. The ICR platform is updated and does not require the use of radioactive materials. The new functional assay provided by this model for NKCC1 enables the accurate ranking of tested compounds and demonstrates its specificity and sensitivity. The Z'-score was calculated to evaluate the robustness of the HTS assay [286]. Afterward, a screening of 1,450 compounds from a targeted library was carried out to identify NKCC1 inhibitors. The automated assay yielded strong results, with a Z' score exceeding 0.7 and demonstrating high consistency across three independent runs. They conducted a full HTS of a library of 1.2 million compounds, with bumetanide included as a positive control. One of the molecules, termed 4636277, was found potent than bumetanide, and another one termed 993437 showed a similar dose-response curve as bumetanide. However, neither of their structures have been released, nor have further in vitro cellular experiments been conducted. Nevertheless, the ICR8000™/ ICR12000™ features an automated sampling mechanism that utilizes microliter sampling technology, making it possible to screen compounds in an HTS format for CCC transporters and beyond.

In silico modeling is the use of computer simulations to model biological systems and predict their behavior. In the context of drug screening, in silico modeling can be used to predict the interactions between potential drug compounds and target proteins. This can save time and resources compared to traditional experimental approaches, as it allows for the quick screening of a vast number of compounds. Among the various methods for screening compounds, HTS using in silico modeling is considered one of the most effective. Other techniques, such as molecular docking and molecular dynamics simulation, are also utilized to assess the absorption, distribution, metabolism, and excretion (ADME) properties. Additionally, for the selected compounds, it is essential to evaluate the ADME properties, carcinogenicity, and toxicological and biological activities (Fig. 8). In 2020, Savardi et al. [223] developed a pharmacophore model using a ligand-based computational approach based on bumetanide and other known inhibitors of NKCC1. The researchers used an iterative way that involved in silico and in vitro screening, along with optimization of small-molecule inhibitor candidates' structural and functional properties to enhance their efficacy. In silico screening was conducted on 135,000 compounds, and subsequently, 255 compounds were examined for NKCC activities using Cl^- influx assay in HEK293 cells. The integrated drug discovery strategy resulted in the identification of two new potential drugs, ARN22642 and ARN22430, which demonstrated strong inhibitory effects on NKCC1 [223]. However, these candidates were found to have poor solubility and metabolic stability. The authors then developed new analogs based on ARN22642 and ARN22430 to address their inadequate drug-like properties. One of these analogs, called ARN23746, was trifluoromethylated and demonstrated significantly improved solubility and metabolic stability, as well as increased potency for inhibiting NKCC1 (31.8% ± 5.4% at 10 µM), and did not exhibit a marked impact on NKCC2 [223]. Inhibition of NKCC1 by ARN23746

restored normal levels of intracellular Cl^- in murine DS neuronal cultures and improved core symptoms in mouse models of autism and DS [223].

In another study, Roy et al. [293] used the predicted human NKCC1 crystal structure to conduct virtual screening of a library of 1,930 brain-permeable compounds using molecular docking. As a result, they discovered four novel NKCC1-selective inhibitors. It is important to conduct both in vitro and in vivo experiments to verify the potency and selectivity of the four identified compounds for NKCC1. Although these compounds have chemical structures that are notably different from bumetanide and other loop diuretics, further testing is required to confirm their effectiveness.

The use of in silico modeling based on available crystal structures of CCCs holds great potential in identifying more promising lead compounds for further testing and development in the future. This can be complemented with other experimental techniques, such as Cryo-EM technology, to offer a comprehensive comprehension of the molecular mechanisms of drug action.

7. Conclusion and future perspectives

In summary, CCCs are transmembrane proteins that have a vital function in the transportation of ions across the cell membrane. These cotransporters participate in the management of intracellular ion concentrations and fluid equilibrium. Additionally, they play a critical part in controlling various physiological functions, including cell volume, blood pressure, neuronal excitability, and more. Each of these cotransporters has a specific role in regulating ion transportation, and their expression and function are regulated by a variety of signaling pathways and physiological stimuli. Deficiencies in CCCs can lead to several diseases and disorders, including epilepsy, cystic fibrosis, Bartter syndrome, and Liddle syndrome. Thus, understanding the way CCCs work and how they are regulated is critical for advancing new treatments for these and other ailments.

Significant research progress has been made in identifying therapeutic indications for these cotransporters in following areas, 1) renal diseases: NKCC2 and NCC have been proven to play important roles in regulating blood pressure and electrolyte balance, making them potential targets for treating various renal diseases, including Bartter's syndrome and Gitelman syndrome; 2) hypertension: blockade of NKCC2 and/or NCC in animal models of hypertension has been found to effectively lower blood pressure; 3) edema: inhibition of NKCC1 has shown promise in reducing edema in animal models of various diseases, including stroke and hydrocephalus; 4) neurological disorders: activation of KCC2 or inhibition of NKCC1, which are involved in regulating neuronal excitability and synaptic plasticity, are potential therapeutic targets for various neurological disorders, such as autism, epilepsy, and neuropathic pain; and 5) cancer: KCC3 and NKCC1 have the potential to be significant factors in the growth and advancement of specific types of cancer, presenting an appealing opportunity to develop novel cancer treatments targeting these proteins. Therefore, it is highly probable that we will observe continuous expansion in the field of CCCs, paving the way for the creation of advanced and potent therapies for a range of diseases in the future.

It is advantageous to have the capability of employing functional assays to identify and describe small-molecule modulators of *SLC12* transporters. Although *SLC12* transporters are electroneutral due to their stoichiometry, the conventional methods available to measure their transport function rely on gauging K^+ or K^+-substitute transport, as well as the direct or indirect assessment of intracellular chloride concentration. Techniques used to evaluate CCC activity include the ammonium pulse technique, radioactive or nonradioactive rubidium ion uptake assay, and Tl^+ uptake assay. Moreover, intracellular chloride concentration can be indirectly assessed using sensitive microelectrodes, radiotracer $^{36}Cl^-$, and fluorescent dyes. Additional techniques for CCC evaluation include looking directly at kinase regulatory sites phosphorylation, flame photometry, $^{22}Na^+$ uptake assay, structural biology, and in silico modeling. To evaluate the activity of KCC2 or NKCC1 in nerve cells, patch-clamp electrophysiology is typically used to measure GABA activity. However, this approach is highly specialized, labor-intensive, and time-consuming, limiting its efficiency and its use for HTS applications. In contrast, the non-radioactive version of the ion flux assay method has shown benefits for studying various types of ion transporters and for conducting high-throughput drug screening. High-resolution structures of CCCs are now available through Cryo-EM technology, enabling researchers to apply in silico modeling for screening more specific and potent CCC compounds. While these cotransporters have shown promise as therapeutic targets in preclinical studies, it is important to note that more research is needed to validate their use in treating human diseases, such as neurological disorders, CVDs, and certain types of cancer.

CRediT author statement

Shiyao Zhang: and **Nur Farah Meor Azlan:** Writing - Original draft preparation, Reviewing and Editing; **Sunday Solomon Josiah** and **Jing Zhou:** Writing - Reviewing and Editing; **Xiaoxia Zhou** and **Lingjun Jie:** Resources, Investigation; **Yanhui Zhang:** Investigation, Supervision; **Cuilian Dai:** Supervision; **Dong Liang:** Resources, Investigation; **Peifeng Li** and **Zhengqiu Li:** Investigation, Supervision; **Zhen Wang:** Resources, Investigation; **Yun Wang:** Supervision, Funding acquisition; **Ke Ding:** Conceptualization, Supervision; **Yan Wang:** Supervision, Project administration, Funding acquisition; **Jinwei Zhang:** Project administration, Supervision, Conceptualization, Validation, Writing - Original draft preparation, Reviewing and Editing, Resources, Funding acquisition.

Declaration of competing interest

Except for Dong Liang, who is an employee of Aurora Discovery Inc., all authors declare that there are no conflicts of interest.

Acknowledgments

Appendix A. Supplementary data

Supplementary data to this article can be found online at https://doi.org/10.1016/j.jpha.2023.09.002.

References

[1] J.C. Venter, M.D. Adams, E.W. Myers, et al., The sequence of the human genome, Science 291 (2001) 1304–1351.
[2] R. Santos, O. Ursu, A. Gaulton, et al., A comprehensive map of molecular drug targets, Nat. Rev. Drug Discov. 16 (2017) 19–34.

[3] D.R. Alessi, J. Zhang, A. Khanna, et al., The WNK-SPAK/OSR1 pathway: Master regulator of cation-chloride cotransporters, Sci. Signal. 7 (2014), re3.

[4] A. Grozio, K.F. Mills, J. Yoshino, et al., Slc12a8 is a nicotinamide mono-nucleotide transporter, Nat. Metab. 1 (2019) 47–57.

[5] N. Ito, A. Takatsu, H. Ito, et al., Slc12a8 in the lateral hypothalamus maintains energy metabolism and skeletal muscle functions during aging, Cell Rep. 40 (2022), 111131.

[6] L. Caron, F. Rousseau, E. Gagnon, et al., Cloning and functional character-ization of a cation-Cl- cotransporter-interacting protein, J. Biol. Chem. 275 (2000) 32027–32036.

[7] T.A. Chew, B.J. Orlando, J. Zhang, et al., Structure and mechanism of the cation-chloride cotransporter NKCC1, Nature 572 (2019) 488–492.

[8] C. Neumann, L.L. Rosenbaek, R.K. Flygaard, et al., Cryo-EM structure of the human NKCC1 transporter reveals mechanisms of ion coupling and speci-ficity, EMBO J. 41 (2022) e110169.

[9] M. Fan, J. Zhang, C.L. Lee, et al., Structure and thiazide inhibition mechanism of the human Na-Cl cotransporter, Nature 614 (2023) 788–793.

[10] J. Nan, Y. Yuan, X. Yang, et al., Cryo-EM structure of the human sodium-chloride cotransporter NCC, Sci. Adv. 8 (2022), eadd7176.

[11] S. Liu, S. Chang, B. Han, et al., Cryo-EM structures of the human cation-chloride cotransporter KCC1, Science 366 (2019) 505–508.

[12] X. Chi, X. Li, Y. Chen, et al., Cryo-EM structures of the full-length human KCC2 and KCC3 cation-chloride cotransporters, Cell Res. 31 (2021) 482–484.

[13] Y. Xie, S. Chang, C. Zhao, et al., Structures and an activation mechanism of human potassium-chloride cotransporters, Sci. Adv. 6 (2020), eabc5883.

[14] M.S. Reid, D.M. Kern, S.G. Brohawn, Cryo-EM structure of the potassium-chloride cotransporter KCC4 in lipid nanodiscs, Elife 9 (2020), e52505.

[15] K. Retterer, J. Juusola, M.T. Cho, et al., Clinical application of whole-exome sequencing across clinical indications, Genet. Med. 18 (2016) 696–704.

[16] T.N. Turner, A.B. Wilfert, T.E. Bakken, et al., Sex-based analysis of de novo variants in neurodevelopmental disorders, Am. J. Hum. Genet. 105 (2019) 1274–1285.

[17] A. Daga, A.J. Majmundar, D.A. Braun, et al., Whole exome sequencing frequently detects a monogenic cause in early onset nephrolithiasis and nephrocalcinosis, Kidney Int. 93 (2018) 204–213.

[18] G. Gamba, A. Miyanoshita, M. Lombardi, et al., Molecular cloning, primary structure, and characterization of two members of the mammalian electro-neutral sodium-(potassium)-chloride cotransporter family expressed in kidney, J. Biol. Chem. 269 (1994) 17713–17722.

[19] J.A. Payne, B. Forbush 3rd, Alternatively spliced isoforms of the putative renal Na-K-Cl cotransporter are differentially distributed within the rabbit kidney, Proc. Natl. Acad. Sci. U S A 91 (1994) 4544–4548.

[20] A. McNeill, E. Iovino, L. Mansard, et al., SLC12A2 variants cause a neuro-developmental disorder or cochleovestibular defect, Brain 143 (2020) 2380–2387.

[21] M. Marchese, G. Valvo, F. Moro, et al., Targeted gene resequencing (astrochip) to explore the tripartite synapse in autism-epilepsy phenotype with mac-rocephaly, Neuromolecular Med. 18 (2016) 69–80.

[22] F. Valentino, L.P. Bruno, G. Doddato, et al., Exome sequencing in 200 intel-lectual disability/autistic patients: New candidates and atypical pre-sentations, Brain Sci. 11 (2021), 936.

[23] N.D. Merner, A. Mercado, A.R. Khanna, et al., Gain-of-function missense variant in SLC12A2, encoding the bumetanide-sensitive NKCC1 cotrans-porter, identified in human schizophrenia, J. Psychiatr. Res. 77 (2016) 22–26.

[24] Y. Morita, J.H. Callicott, L.R. Testa, et al., Characteristics of the cation cotransporter NKCC1 in human brain: Alternate transcripts, expression in development, and potential relationships to brain function and schizo-phrenia, J. Neurosci. 34 (2014) 4929–4940.

[25] S. Anazi, S. Maddirevula, V. Salpietro, et al., Expanding the genetic hetero-geneity of intellectual disability, Hum. Genet. 136 (2017) 1419–1429.

[26] E.F. Macnamara, A.E. Koehler, P. D'Souza, et al., Kilquist syndrome: A novel syndromic hearing loss disorder caused by homozygous deletion of SLC12A2, Hum. Mutat. 40 (2019) 532–538.

[27] T. Stödberg, M. Magnusson, N. Lesko, et al., SLC12A2 mutations cause NKCC1 deficiency with encephalopathy and impaired secretory epithelia, Neurol. Genet. 6 (2020), e478.

[28] H. Mutai, K. Wasano, Y. Momozawa, et al., Variants encoding a restricted carboxy-terminal domain of SLC12A2 cause hereditary hearing loss in humans, PLoS Genet. 16 (2020), e1008643.

[29] R.L.P. Santos-Cortez, T.K.L. Yarza, T.C. Bootpetch, et al., Identification of novel candidate genes and variants for hearing loss and temporal bone anomalies, Genes (Basel) 12 (2021), 566.

[30] S.M. Adadey, I. Schrauwen, E.T. Aboagye, et al., Further confirmation of the association of SLC12A2 with non-syndromic autosomal-dominant hearing impairment, J. Hum. Genet. 66 (2021) 1169–1175.

[31] Y. Liu, X. Chang, J. Glessner, et al., Association of rare recurrent copy number variants with congenital heart defects based on next-generation sequencing data from family trios, Front. Genet. 10 (2019), 819.

[32] E. Delpire, M.I. Rauchman, D.R. Beier, et al., Molecular cloning and chromo-some localization of a putative basolateral Na+-K+-2Cl− cotransporter from mouse inner medullary collecting duct (mIMCD-3) cells, J. Biol. Chem. 269 (1994) 25677–25683.

[33] J.-C. Xu, C. Lytle, T.-T. Zhu, et al., Molecular cloning and functional expression of the bumetanide-sensitive Na-K-Cl cotransporter, Proc. Natl. Acad. Sci. U S A 91 (1994) 2201–2205.

[34] Z. Huang, Y. Sun, Y. Fan, et al., Genetic evaluation of 114 Chinese short stature children in the next generation era: A single center study, Cell. Physiol. Biochem. 49 (2018) 295–305.

[35] N. Tanaka, T. Babazono, S. Saito, et al., Association of solute carrier family 12 (sodium/chloride) member 3 with diabetic nephropathy, identified by genome-wide analyses of single nucleotide polymorphisms, Diabetes 52 (2003) 2848–2853.

[36] F.E. Dewey, M.F. Murray, J.D. Overton, et al., Distribution and clinical impact of functional variants in 50,726 whole-exome sequences from the DiscovEHR study, Science 354 (2016), aaf6814.

[37] G. Gamba, S.N. Saltzberg, M. Lombardi, et al., Primary structure and functional expression of a cDNA encoding the thiazide-sensitive, electroneutral sodium-chloride cotransporter, Proc. Natl. Acad. Sci. U S A 90 (1993) 2749–2753.

[38] I. Iossifov, B.J. O'Roak, S.J. Sanders, et al., The contribution of de novo coding mutations to autism spectrum disorder, Nature 515 (2014) 216–221.

[39] E.T. Lim, M. Uddin, S. De Rubeis, et al., Rates, distribution and implications of postzygotic mosaic mutations in autism spectrum disorder, Nat. Neurosci. 20 (2017) 1217–1224.

[40] D.N. Subramanian, M. Zethoven, S. McInerny, et al., Exome sequencing of familial high-grade serous ovarian carcinoma reveals heterogeneity for rare candidate susceptibility genes, Nat. Commun. 11 (2020), 1640.

[41] J.C. Ulirsch, S.K. Nandakumar, L. Wang, et al., Systematic functional dissection of common genetic variation affecting red blood cell traits, Cell 165 (2016) 1530–1545.

[42] L. Southgate, M. Sukalo, A.S.V. Karountzos, et al., Haploinsufficiency of the NOTCH1 receptor as a cause of Adams-Oliver syndrome with variable cardiac anomalies, Circ. Cardiovasc. Genet. 8 (2015) 572–581.

[43] C.M. Gillen, S. Brill, J.A. Payne, et al., Molecular cloning and functional expression of the K-Cl cotransporter from rabbit, rat, and human. A new member of the cation-chloride cotransporter family, J. Biol. Chem. 271 (1996) 16237–16244.

[44] H. Saitsu, M. Watanabe, T. Akita, et al., Impaired neuronal KCC2 function by biallelic SLC12A5 mutations in migrating focal seizures and severe devel-opmental delay, Sci. Rep. 6 (2016), 30072.

[45] T. Stödberg, A. McTague, A.J. Ruiz, et al., Mutations in SLC12A5 in epilepsy of infancy with migrating focal seizures, Nat. Commun. 6 (2015), 8038.

[46] K.T. Kahle, N.D. Merner, P. Friedel, et al., Genetically encoded impairment of neuronal KCC2 cotransporter function in human idiopathic generalized ep-ilepsy, EMBO Rep. 15 (2014) 766–774.

[47] M. Puskarjov, P. Seja, S.E. Heron, et al., A variant of KCC2 from patients with febrile seizures impairs neuronal Cl− extrusion and dendritic spine forma-tion, EMBO Rep. 15 (2014) 723–729.

[48] S.L. Campbell, S. Robel, V.A. Cuddapah, et al., GABAergic disinhibition and impaired KCC2 cotransporter activity underlie tumor-associated epilepsy, Glia 63 (2015) 23–36.

[49] J.A. Kosmicki, K.E. Samocha, D.P. Howrigan, et al., Refining the role of de novo protein-truncating variants in neurodevelopmental disorders by using population reference samples, Nat. Genet. 49 (2017) 504–510.

[50] N.D. Merner, M.R. Chandler, C. Bourassa, et al., Regulatory domain or CpG site variation in SLC12A5, encoding the chloride transporter KCC2, in human autism and schizophrenia, Front. Cell. Neurosci. 9 (2015), 386.

[51] J.A. Payne, T.J. Stevenson, L.F. Donaldson, Molecular characterization of a putative K-Cl cotransporter in rat brain. A neuronal-specific isoform, J. Biol. Chem. 271 (1996) 16245–16252.

[52] T. Antoniadi, C. Buxton, G. Dennis, et al., Application of targeted multi-gene panel testing for the diagnosis of inherited peripheral neuropathy provides a high diagnostic yield with unexpected phenotype-genotype variability, BMC Med. Genet. 16 (2015), 84.

[53] G. Uyanik, N. Elcioglu, J. Penzien, et al., Novel truncating and missense mu-tations of the KCC3 gene associated with Andermann syndrome, Neurology 66 (2006) 1044–1048.

[54] K.T. Kahle, B. Flores, D. Bharucha-Goebel, et al., Peripheral motor neuropathy is associated with defective kinase regulation of the KCC3 cotransporter, Sci. Signal. 9 (2016), ra77.

[55] C.M. Lourenço, N. Dupré, J.B. Rivière, et al., Expanding the differential diag-nosis of inherited neuropathies with non-uniform conduction: Andermann syndrome, J. Peripher. Nerv. Syst. 17 (2012) 123–127.

[56] Y.-C. Hou, H.-C. Yu, R. Martin, et al., Precision medicine integrating whole-genome sequencing, comprehensive metabolomics, and advanced imaging, Proc. Natl. Acad. Sci. U S A 117 (2020) 3053–3062.

[57] M. Shekarabi, R.X. Moldrich, S. Rasheed, et al., Loss of neuronal potassium/chloride cotransporter 3 (KCC3) is responsible for the degenerative pheno-type in a conditional mouse model of hereditary motor and sensory neu-ropathy associated with agenesis of the corpus callosum, J. Neurosci. 32 (2012) 3865–3876.

[58] K. Hiki, R.J. D'Andrea, J. Furze, et al., Cloning, characterization, and chromo-somal location of a novel human K+-Cl− cotransporter, J. Biol. Chem. 274 (1999) 10661–10667.

[59] J.E. Race, F.N. Makhlouf, P.J. Logue, et al., Molecular cloning and functional characterization of KCC3, a new K-Cl cotransporter, Am. J. Physiol. 277 (1999) C1210–C1219.

[60] D.B. Mount, A. Mercado, L. Song, et al., Cloning and characterization of KCC3 and KCC4, new members of the cation-chloride cotransporter gene family, J. Biol. Chem. 274 (1999) 16355–16362.

[61] A. Takata, M. Nakashima, H. Saitsu, et al., Comprehensive analysis of coding variants highlights genetic complexity in developmental and epileptic encephalopathy, Nat. Commun. 10 (2019), 2506.

[62] S.C. Jin, C.G. Furey, X. Zeng, et al., SLC12A ion transporter mutations in sporadic and familial human congenital hydrocephalus, Mol. Genet. Genomic Med. 7 (2019), e892.

[63] D. Hewett, L. Samuelsson, J. Polding, et al., Identification of a psoriasis susceptibility candidate gene by linkage disequilibrium mapping with a localized single nucleotide polymorphism map, Genomics 79 (2002) 305–314.

[64] J.J. Edwards, A.D. Rouillard, N.F. Fernandez, et al., Systems analysis implicates WAVE2 complex in the pathogenesis of developmental left-sided obstructive heart defects, JACC Basic Transl. Sci. 5 (2020) 376–386.

[65] D.B. Mount, A. Baekgaard, A.E. Hall, et al., Isoforms of the Na-K-2Cl cotransporter in murine TAL I. Molecular characterization and intrarenal localization, Am. J. Physiol. 276 (1999) F347–F358.

[66] D.B. Simon, F.E. Karet, J.M. Hamdan, et al., Bartter's syndrome, hypokalaemic alkalosis with hypercalciuria, is caused by mutations in the Na-K-2Cl cotransporter NKCC2, Nat. Genet. 13 (1996) 183–188.

[67] S.M. Robert, B.C. Reeves, E. Kiziltug, et al., The choroid plexus links innate immunity to CSF dysregulation in hydrocephalus, Cell 186 (2023) 764–785.

[68] J. Zhang, Gitelman syndrome. N. Rezaei, Genetic Syndromes: A Comprehensive Reference Guide, first ed., Springer Nature, Switzerland, 2023, pp. 1–4.

[69] F.C. Brown, A.J. Conway, L. Cerruti, et al., Activation of the erythroid K-Cl cotransporter Kcc1 enhances sickle cell disease pathology in a humanized mouse model, Blood 126 (2015) 2863–2870.

[70] T.Q. Vu, J.A. Payne, D.R. Copenhagen, Localization and developmental expression patterns of the neuronal K-Cl cotransporter (KCC2) in the rat retina, J. Neurosci. 20 (2000) 1414–1423.

[71] M. Heubl, J. Zhang, J.C. Pressey, et al., GABA$_A$ receptor dependent synaptic inhibition rapidly tunes KCC2 activity via the Cl$^-$-sensitive WNK1 kinase, Nat. Commun. 8 (2017), 1776.

[72] M. Watanabe, J. Zhang, M.S. Mansuri, et al., Developmentally regulated KCC2 phosphorylation is essential for dynamic GABA-mediated inhibition and survival, Sci. Signal. 12 (2019), eaaw9315.

[73] S. Salihu, N.F. Meor Azlan, S.S. Josiah, et al., Role of the cation-chloride-cotransporters in the circadian system, Asian J. Pharm. Sci. 16 (2021) 589–597.

[74] C. Shimizu-Okabe, S. Okada, S. Okamoto, et al., Specific expression of KCC2 in the α cells of normal and type 1 diabetes model mouse pancreatic islets, Acta Histochem. Cytochem. 55 (2022) 47–56.

[75] S. Kursan, T.S. McMillen, P. Beesetty, et al., The neuronal K$^+$Cl$^-$ co-transporter 2 (Slc12a5) modulates insulin secretion, Sci. Rep. 7 (2017), 1732.

[76] H.C. Howard, D.B. Mount, D. Rochefort, et al., The K-Cl cotransporter KCC3 is mutant in a severe peripheral neuropathy associated with agenesis of the corpus callosum, Nat. Genet. 32 (2002) 384–392.

[77] R. Rius, A. Gonzalez-Del Angel, J.A. Velázquez-Aragón, et al., Identification of a novel *SLC12A6* pathogenic variant associated with hereditary motor and sensory neuropathy with agenesis of the corpus callosum (HMSN/ACC) in a non-French-Canadian family, Neurol. India 66 (2018) 1162–1165.

[78] T. Muñoz, P. Krishnan, J. Vajsar, et al., Andermann syndrome in a Pakistani family caused by a novel mutation in SLC12A6, J. Pediatr. Neurol. 15 (2017) 90–94.

[79] T. Boettger, C.A. Hübner, H. Maier, et al., Deafness and renal tubular acidosis in mice lacking the K-Cl co-transporter Kcc4, Nature 416 (2002) 874–878.

[80] N.D. Daigle, G.A. Carpentier, R. Frenette-Cotton, et al., Molecular characterization of a human cation-Cl- cotransporter (SLC12A8A, CCC9A) that promotes polyamine and amino acid transport, J. Cell. Physiol. 220 (2009) 680–689.

[81] M. Wenz, A.M. Hartmann, E. Friauf, et al., CIP1 is an activator of the K$^+$-Cl$^-$ cotransporter KCC2, Biochem. Biophys. Res. Commun. 381 (2009) 388–392.

[82] C. Rivera, J. Voipio, J.A. Payne, et al., The K$^+$/Cl$^-$ co-transporter KCC2 renders GABA hyperpolarizing during neuronal maturation, Nature 397 (1999) 251–255.

[83] A. Bertoni, F. Schaller, R. Tyzio, et al., Oxytocin administration in neonates shapes hippocampal circuitry and restores social behavior in a mouse model of autism, Mol. Psychiatry 26 (2021) 7582–7595.

[84] K.T. Kahle, J.F. Schmouth, V. Lavastre, et al., Inhibition of the kinase WNK1/HSN2 ameliorates neuropathic pain by restoring GABA inhibition, Sci. Signal. 9 (2016), ra32.

[85] Y. Belaïdouni, D. Diabira, J. Zhang, et al., The chloride homeostasis of CA3 hippocampal neurons is not altered in fully symptomatic *Mepc2-null* mice, Front. Cell. Neurosci. 15 (2021), 724976.

[86] F. Galeffi, R. Sah, B.B. Pond, et al., Changes in intracellular chloride after oxygen-glucose deprivation of the adult hippocampal slice: Effect of diazepam, J. Neurosci. 24 (2004) 4478–4488.

[87] E. Papp, C. Rivera, K. Kaila, et al., Relationship between neuronal vulnerability and potassium-chloride cotransporter 2 immunoreactivity in hippocampus following transient forebrain ischemia, Neuroscience 154 (2008) 677–689.

[88] F. Wang, X. Wang, L.A. Shapiro, et al., NKCC1 up-regulation contributes to early post-traumatic seizures and increased post-traumatic seizure susceptibility, Brain Struct. Funct. 222 (2017) 1543–1556.

[89] C. Brandt, M. Nozadze, N. Heuchert, et al., Disease-modifying effects of phenobarbital and the NKCC1 inhibitor bumetanide in the pilocarpine model of temporal lobe epilepsy, J. Neurosci. 30 (2010) 8602–8612.

[90] Y. Gong, M. Wu, J. Shen, et al., Inhibition of the NKCC1/NF-κB signaling pathway decreases inflammation and improves brain edema and nerve cell apoptosis in an SBI rat model, Front. Mol. Neurosci. 14 (2021), 641993.

[91] J. Wang, R. Liu, M.N. Hasan, et al., Role of SPAK-NKCC1 signaling cascade in the choroid plexus blood-CSF barrier damage after stroke, J. Neuroinflammation 19 (2022), 91.

[92] J.K. Karimy, J. Zhang, D.B. Kurland, et al., Inflammation-dependent cerebrospinal fluid hypersecretion by the choroid plexus epithelium in posthemorrhagic hydrocephalus, Nat. Med. 23 (2017) 997–1003.

[93] J. Zhang, H. Pu, H. Zhang, et al., Inhibition of Na$^+$-K$^+$-2Cl$^-$ cotransporter attenuates blood-brain-barrier disruption in a mouse model of traumatic brain injury, Neurochem. Int. 111 (2017) 23–31.

[94] S.-R. Chen, L. Zhu, H. Chen, et al., Increased spinal cord Na$^+$-K$^+$-2Cl$^-$ cotransporter-1 (NKCC1) activity contributes to impairment of synaptic inhibition in paclitaxel-induced neuropathic pain, J. Biol. Chem. 289 (2014) 31111–31120.

[95] Y. Wu, F. Wang, Inhibition of NKCC1 in spinal dorsal horn and dorsal root ganglion results in alleviation of neuropathic pain in rats with spinal cord contusion, Mol. Pain 19 (2023), 17448069231159855.

[96] L. Michea, V. Irribarra, I.A. Goecke, et al., Reduced Na-K pump but increased Na-K-2Cl cotransporter in aorta of streptozotocin-induced diabetic rat, Am. J. Physiol. Heart Circ. Physiol. 280 (2001) H851–H858.

[97] M. Ji, S. In Lee, S.A. Lee, et al., Enhanced activity by NKCC1 and Slc26a6 mediates acidic pH and Cl$^-$ movement after cardioplegia-induced arrest of db/db diabetic heart, Mediators Inflamm. 2019 (2019), 7583760.

[98] S.V. Koltsova, S.V. Kotelevtsev, J. Tremblay, et al., Excitation-contraction coupling in resistance mesenteric arteries: Evidence for NKCC1-mediated pathway, Biochem. Biophys. Res. Commun. 379 (2009) 1080–1083.

[99] M. Di Fulvio, T.M. Lincoln, P.K. Lauf, et al., Protein kinase G regulates potassium chloride cotransporter-3 expression in primary cultures of rat vascular smooth muscle cells, J. Biol. Chem. 276 (2001) 21046–21052.

[100] A.P. Garneau, A.A. Marcoux, M. Noël, et al., Ablation of potassium-chloride cotransporter type 3 (Kcc3) in mouse causes multiple cardiovascular defects and isosmotic polyuria, PLoS One 11 (2016), e0154398.

[101] M. Di Fulvio, P.K. Lauf, S. Shah, et al., NONOates regulate KCl cotransporter-1 and -3 mRNA expression in vascular smooth muscle cells, Am. J. Physiol. Heart Circ. Physiol. 284 (2003) H1686–H1692.

[102] J. Zhang, P.K. Lauf, N.C. Adragna, Platelet-derived growth factor regulates K-Cl cotransport in vascular smooth muscle cells, Am. J. Physiol. Cell Physiol. 284 (2003) C674–C680.

[103] F.H. Wilson, S. Disse-Nicodème, K.A. Choate, et al., Human hypertension caused by mutations in WNK kinases, Science 293 (2001) 1107–1112.

[104] L.M. Boyden, M. Choi, K.A. Choate, et al., Mutations in kelch-like 3 and cullin 3 cause hypertension and electrolyte abnormalities, Nature 482 (2012) 98–102.

[105] M. Castañeda-Bueno, L.G. Cervantes-Pérez, N. Vázquez, et al., Activation of the renal Na$^+$:Cl$^-$ cotransporter by angiotensin II is a WNK4-dependent process, Proc. Natl. Acad. Sci. U S A 109 (2012) 7929–7934.

[106] F.R. Schumacher, K. Siew, J. Zhang, et al., Characterisation of the Cullin-3 mutation that causes a severe form of familial hypertension and hyperkalaemia, EMBO Mol. Med. 7 (2015) 1285–1306.

[107] M. Ostrosky-Frid, M. Chávez-Canales, J. Zhang, et al., Role of KLHL3 and dietary K$^+$ in regulating KS-WNK1 expression, Am. J. Physiol. Renal Physiol. 320 (2021) F734–F747.

[108] D. Takahashi, T. Mori, N. Nomura, et al., WNK4 is the major WNK positively regulating NCC in the mouse kidney, Biosci. Rep. 34 (2014), e00107.

[109] J. Zhang, K. Siew, T. Macartney, et al., Critical role of the SPAK protein kinase CCT domain in controlling blood pressure, Hum. Mol. Genet. 24 (2015) 4545–4558.

[110] K. Yamada, H.M. Park, D.F. Rigel, et al., Small-molecule WNK inhibition regulates cardiovascular and renal function, Nat. Chem. Biol. 12 (2016) 896–898.

[111] N.F. Meor Azlan, J. Zhang, Role of the cation-chloride-cotransporters in cardiovascular disease, Cells 9 (2020), 2293.

[112] R. Panet, M. Marcus, H. Atlan, Overexpression of the Na$^+$/K$^+$/Cl$^-$ cotransporter gene induces cell proliferation and phenotypic transformation in mouse fibroblasts, J. Cell. Physiol. 182 (2000) 109–118.

[113] P.-L. Sun, Y. Jin, S.Y. Park, et al., Expression of Na$^+$-K$^+$-2Cl$^-$ cotransporter isoform 1 (NKCC1) predicts poor prognosis in lung adenocarcinoma and EGFR-mutated adenocarcinoma patients, QJM 109 (2016) 237–244.

[114] J.-F. Wang, K. Zhao, Y.-Y. Chen, et al., NKCC1 promotes proliferation, invasion and migration in human gastric cancer cells via activation of the MAPK-JNK/EMT signaling pathway, J. Cancer 12 (2021) 253–263.

[115] K. Hiraoka, H. Miyazaki, N. Niisato, et al., Chloride ion modulates cell proliferation of human androgen-independent prostatic cancer cell, Cell. Physiol. Biochem. 25 (2010) 379—388.

[116] A. Shiozaki, Y. Nako, D. Ichikawa, et al., Role of the Na$^+$/K$^+$/2Cl$^-$ cotransporter NKCC1 in cell cycle progression in human esophageal squamous cell carcinoma, World J. Gastroenterol. 20 (2014) 6844—6859.

[117] L. Luo, X. Guan, G. Begum, et al., Blockade of cell volume regulatory protein NKCC1 increases TMZ-induced glioma apoptosis and reduces astrogliosis, Mol. Cancer Ther. 19 (2020) 1550—1561.

[118] S. Zhang, X. Wu, T. Jiang, et al., The up-regulation of KCC1 gene expression in cervical cancer cells by IGF-II through the ERK1/2MAPK and PI3K/AKT pathways and its significance, Eur. J. Gynaecol. Oncol. 30 (2009) 29—34.

[119] H. Kajiya, F. Okamoto, J.-P. Li, et al., Expression of mouse osteoclast K-Cl cotransporter-1 and its role during bone resorption, J. Bone Miner. Res. 21 (2006) 984—992.

[120] M.-R. Shen, C.-Y. Chou, K.-F. Hsu, et al., The KCl cotransporter isoform KCC3 can play an important role in cell growth regulation, Proc. Natl. Acad. Sci. U S A 98 (2001) 14714—14719.

[121] M.B. Rust, S.L. Alper, Y. Rudhard, et al., Disruption of erythroid K-Cl cotransporters alters erythrocyte volume and partially rescues erythrocyte dehydration in SAD mice, J. Clin. Invest. 117 (2007) 1708—1717.

[122] H.F. Clemo, J.J. Feher, C.M. Baumgarten, Modulation of rabbit ventricular cell volume and Na$^+$/K$^+$/2Cl$^-$ cotransport by cGMP and atrial natriuretic factor, J. Gen. Physiol. 100 (1992) 89—114.

[123] G. Gamba, Molecular physiology and pathophysiology of electroneutral cation-chloride cotransporters, Physiol. Rev. 85 (2005) 423—493.

[124] Y. Okada, Ion channels and transporters involved in cell volume regulation and sensor mechanisms, Cell Biochem. Biophys. 41 (2004) 233—258.

[125] C.-P. Zhao, H.-Y. Guo, K.-C. Zhu, et al., Molecular characterization of Na$^+$/K$^+$/2Cl$^-$ cotransporter 1 alpha from *Trachinotus ovatus* (Linnaeus, 1758) and its expression responses to acute salinity stress, Comp. Biochem. Physiol. B Biochem. Mol. Biol. 223 (2018) 29—38.

[126] R.T. Alexander, S. Grinstein, Na$^+$/H$^+$ exchangers and the regulation of volume, Acta Physiol. (Oxf.) 187 (2006) 159—167.

[127] S. Grinstein, C.A. Clarke, A. Rothstein, Activation of Na$^+$/H$^+$ exchange in lymphocytes by osmotically induced volume changes and by cytoplasmic acidification, J. Gen. Physiol. 82 (1983) 619—638.

[128] M. Song, S.P. Yu, Ionic regulation of cell volume changes and cell death after ischemic stroke, Transl. Stroke Res. 5 (2014) 17—27.

[129] A. Qusous, C.S. Geewan, P. Greenwell, et al., siRNA-mediated inhibition of Na$^+$-K$^+$-2Cl$^-$ cotransporter (NKCC1) and regulatory volume increase in the chondrocyte cell line C-20/A4, J. Membr. Biol. 243 (2011) 25—34.

[130] N.C. Adragna, N.B. Ravilla, P.K. Lauf, et al., Regulated phosphorylation of the K-Cl cotransporter KCC3 is a molecular switch of intracellular potassium content and cell volume homeostasis, Front. Cell. Neurosci. 9 (2015), 255.

[131] M.A. Tejada, K. Stople, S. Hammami Bomholtz, et al., Cell volume changes regulate slick (Slo2.1), but not slack (Slo2.2) K$^+$ channels, PLoS One 9 (2014), e110833.

[132] L. Sforna, A. Michelucci, F. Morena, et al., Piezo1 controls cell volume and migration by modulating swelling-activated chloride current through Ca^{2+} influx, J. Cell. Physiol. 237 (2022) 1857—1870.

[133] E.K. Hoffmann, I.H. Lambert, S.F. Pedersen, Physiology of cell volume regulation in vertebrates, Physiol. Rev. 89 (2009) 193—277.

[134] P. de Los Heros, D.R. Alessi, R. Gourlay, et al., The WNK-regulated SPAK/OSR1 kinases directly phosphorylate and inhibit the K$^+$-Cl$^-$ co-transporters, Biochem. J. 458 (2014) 559—573.

[135] C. Richardson, F.H. Rafiqi, H.K. Karlsson, et al., Activation of the thiazide-sensitive Na$^+$-Cl$^-$ cotransporter by the WNK-regulated kinases SPAK and OSR1, J. Cell Sci. 121 (2008) 675—684.

[136] K.T. Kahle, J. Rinehart, P. de Los Heros, et al., WNK3 modulates transport of Cl$^-$ in and out of cells: Implications for control of cell volume and neuronal excitability, Proc. Natl. Acad. Sci. U S A 102 (2005) 16783—16788.

[137] C.R. Boyd-Shiwarski, D.J. Shiwarski, S.E. Griffiths, et al., WNK kinases sense molecular crowding and rescue cell volume via phase separation, Cell 185 (2022) 4488—4506.e20.

[138] J. Zhang, M.I.H. Bhuiyan, T. Zhang, et al., Modulation of brain cation-Cl$^-$ cotransport via the SPAK kinase inhibitor ZT-1a, Nat. Commun. 11 (2020), 78.

[139] V.N. Bildin, Z. Wang, P. Iserovich, et al., Hypertonicity-induced p38MAPK activation elicits recovery of corneal epithelial cell volume and layer integrity, J. Membr. Biol. 193 (2003) 1—13.

[140] G. Scepanovic, M.V. Hunter, R. Kafri, et al., p38-mediated cell growth and survival drive rapid embryonic wound repair, Cell Rep. 37 (2021), 109874.

[141] L. Mòdol, D. Santos, S. Cobianchi, et al., NKCC1 activation is required for myelinated sensory neurons regeneration through JNK-dependent pathway, J. Neurosci. 35 (2015) 7414—7427.

[142] E.K. Hoffmann, S.F. Pedersen, Shrinkage insensitivity of NKCC1 in myosin II-depleted cytoplasts from Ehrlich ascites tumor cells, Am. J. Physiol. Cell Physiol. 292 (2007) C1854—C1866.

[143] W.L. Demian, A. Persaud, C. Jiang, et al., The ion transporter NKCC1 links cell volume to cell mass regulation by suppressing mTORC1, Cell Rep. 27 (2019) 1886—1896.e6.

[144] S.A. Serra, P. Stojakovic, R. Amat, et al., LRRC8A-containing chloride channel is crucial for cell volume recovery and survival under hypertonic conditions, Proc. Natl. Acad. Sci. U S A 118 (2021), e2025013118.

[145] M.A. Model, Methods for cell volume measurement, Cytometry A 93 (2018) 281—296.

[146] S. Mizutani, S.M. Prasad, A.D. Sellitto, et al., Myocyte volume and function in response to osmotic stress: Observations in the presence of an adenosine triphosphate-sensitive potassium channel opener, Circulation 112 (2005) I219—I223.

[147] S. Liu, M.B. Ginzberg, N. Patel, et al., Size uniformity of animal cells is actively maintained by a p38 MAPK-dependent regulation of G1-length, Elife 7 (2018), e26947.

[148] R. Munns, P.A. Wallace, N.L. Teakle, et al., Measuring soluble ion concentrations (Na$^+$, K$^+$, Cl$^-$) in salt-treated plants. R. Sunkar Plant Stress Tolerance, first ed., Vol. 639, Humana Press, Totowa, NJ, 2010, pp. 371—382.

[149] M. Haas, The Na-K-Cl cotransporters, Am. J. Physiol. 267 (1994) C869—C885.

[150] S. Bazúa-Valenti, L. Rojas-Vega, M. Castañeda-Bueno, et al., The calcium-sensing receptor increases activity of the renal NCC through the WNK4-SPAK pathway, J. Am. Soc. Nephrol. 29 (2018) 1838—1848.

[151] F.A. Gesek, P.A. Friedman, Mechanism of calcium transport stimulated by chlorothiazide in mouse distal convoluted tubule cells, J. Clin. Invest. 90 (1992) 429—438.

[152] R.S. Hoover, E. Poch, A. Monroy, et al., *N*-glycosylation at two sites critically alters thiazide binding and activity of the rat thiazide-sensitive Na$^+$:Cl$^-$ cotransporter, J. Am. Soc. Nephrol. 14 (2003) 271—282.

[153] G. Gamba, Regulation of the renal Na$^+$-Cl$^-$ cotransporter by phosphorylation and ubiquitylation, Am. J. Physiol. Renal Physiol. 303 (2012) F1573—F1583.

[154] L.L. Rosenbaek, F. Rizzo, N. MacAulay, et al., Functional assessment of sodium chloride cotransporter NCC mutants in polarized mammalian epithelial cells, Am. J. Physiol. Renal Physiol. 313 (2017) F495—F504.

[155] G.C. Terstappen, Nonradioactive rubidium ion efflux assay and its applications in drug discovery and development, Assay Drug Dev. Technol. 2 (2004) 553—559.

[156] J.R. Williams, J.A. Payne, Cation transport by the neuronal K$^+$-Cl$^-$ cotransporter KCC2: Thermodynamics and kinetics of alternate transport modes, Am. J. Physiol. Cell Physiol. 287 (2004) C919—C931.

[157] E. Chorin, O. Vinograd, I. Fleidervish, et al., Upregulation of KCC2 activity by zinc-mediated neurotransmission via the mZnR/GPR39 receptor, J. Neurosci. 31 (2011) 12916—12926.

[158] S. Titz, S. Hormuzdi, A. Lewen, et al., Intracellular acidification in neurons induced by ammonium depends on KCC2 function, Eur. J. Neurosci. 23 (2006) 454—464.

[159] M. Hershfinkel, K. Kandler, M.E. Knoch, et al., Intracellular zinc inhibits KCC2 transporter activity, Nat. Neurosci. 12 (2009) 725—727.

[160] E. Vizvári, M. Katona, P. Orvos, et al., Characterization of Na$^+$-K$^+$-2Cl$^-$ cotransporter activity in rabbit lacrimal gland duct cells, Invest. Ophthalmol. Vis. Sci. 57 (2016) 3828—3835.

[161] D. Heitzmann, R. Warth, M. Bleich, et al., Regulation of the Na$^+$2Cl$^-$K$^+$ cotransporter in isolated rat colon crypts, Pflugers Arch. 439 (2000) 378—384.

[162] M. Kidokoro, T. Nakamoto, T. Mukaibo, et al., Na$^+$ -K$^+$ -2Cl$^-$ cotransporter-mediated fluid secretion increases under hypotonic osmolarity in the mouse submandibular salivary gland, Am. J. Physiol. Renal Physiol. 306 (2014) F1155—F1160.

[163] I. Medina, P. Friedel, C. Rivera, et al., Current view on the functional regulation of the neuronal K$^+$-Cl$^-$ cotransporter KCC2, Front. Cell. Neurosci. 8 (2014), 27.

[164] G.C. Terstappen, Nonradioactive rubidium efflux assay technology for screening of ion channels. M.A. Cooper, L. Mayr, Label-free technologies for Drug Discovery, first ed., John Wiley & Sons, Chichester, West Sussex, 2011, pp. 111—122.

[165] M. Carmosino, F. Rizzo, S. Torretta, et al., High-throughput fluorescent-based NKCC functional assay in adherent epithelial cells, BMC Cell Biol. 14 (2013), 16.

[166] S.A. Titus, D. Beacham, S.A. Shahane, et al., A new homogeneous high-throughput screening assay for profiling compound activity on the human ether-a-go-go-related gene channel, Anal. Biochem. 394 (2009) 30—38.

[167] D.W. Beacham, T. Blackmer, M. O'Grady, et al., Cell-based potassium ion channel screening using the FluxOR assay, J. Biomol. Screen. 15 (2010) 441—446.

[168] E. Delpire, E. Days, L.M. Lewis, et al., Small-molecule screen identifies inhibitors of the neuronal K-Cl cotransporter KCC2, Proc. Natl. Acad. Sci. U S A 106 (2009) 5383—5388.

[169] D. Zhang, S.M. Gopalakrishnan, G. Freiberg, et al., A thallium transport FLIPR-based assay for the identification of KCC2-positive modulators, J. Biomol. Screen. 15 (2010) 177—184.

[170] S. Zhang, J. Zhou, Y. Zhang, et al., The structural basis of function and regulation of neuronal cotransporters NKCC1 and KCC2, Commun. Biol. 4 (2021), 226.

[171] H.-B. Yu, M. Li, W.-P. Wang, et al., High throughput screening technologies for ion channels, Acta Pharmacol. Sin. 37 (2016) 34—43.

[172] C.L. Hill, G.J. Stephens, An introduction to patch clamp recording, Methods Mol. Biol. 2188 (2021) 1—19.

[173] H.H. Lee, T.Z. Deeb, J.A. Walker, et al., NMDA receptor activity downregulates KCC2 resulting in depolarizing GABA$_A$ receptor-mediated currents, Nat. Neurosci. 14 (2011) 736–743.

[174] M.A. Woodin, K. Ganguly, M.M. Poo, Coincident pre- and postsynaptic activity modifies GABAergic synapses by postsynaptic changes in Cl$^-$ transporter activity, Neuron 39 (2003) 807–820.

[175] P. Friedel, K.T. Kahle, J. Zhang, et al., WNK1-regulated inhibitory phosphorylation of the KCC2 cotransporter maintains the depolarizing action of GABA in immature neurons, Sci. Signal. 8 (2015), ra65.

[176] R.A. Cardarelli, K. Jones, L.I. Pisella, et al., The small molecule CLP257 does not modify activity of the K$^+$-Cl$^-$ co-transporter KCC2 but does potentiate GABA$_A$ receptor activity, Nat. Med. 23 (2017) 1394–1396.

[177] K.L. Lee, K. Abiraman, C. Lucaj, et al., Inhibiting with-no-lysine kinases enhances K$^+$/Cl$^-$ cotransporter 2 activity and limits status epilepticus, Brain 145 (2022) 950–963.

[178] S. Ebihara, K. Shirato, N. Harata, et al., Gramicidin-perforated patch recording: GABA response in mammalian neurones with intact intracellular chloride, J. Physiol. 484 (Pt 1) (1995) 77–86.

[179] K. Lamsa, J.M. Palva, E. Ruusuvuori, et al., Synaptic GABA$_A$ activation inhibits AMPA-kainate receptor-mediated bursting in the newborn (P0–P2) rat hippocampus, J. Neurophysiol. 83 (2000) 359–366.

[180] A. Kyrozis, D.B. Reichling, Perforated-patch recording with gramicidin avoids artifactual changes in intracellular chloride concentration, J. Neurosci. Methods 57 (1995) 27–35.

[181] C. Lytle, B. Forbush 3rd, Regulatory phosphorylation of the secretory Na-K-Cl cotransporter: Modulation by cytoplasmic Cl, Am. J. Physiol. 270 (1996) C437–C448.

[182] R.B. Darman, B. Forbush, A regulatory locus of phosphorylation in the N terminus of the Na-K-Cl cotransporter, NKCC1, J. Biol. Chem. 277 (2002) 37542–37550.

[183] M. Mann, S.E. Ong, M. Grønborg, et al., Analysis of protein phosphorylation using mass spectrometry: Deciphering the phosphoproteome, Trends Biotechnol. 20 (2002) 261–268.

[184] J.J. Pitt, Principles and applications of liquid chromatography-mass spectrometry in clinical biochemistry, Clin. Biochem. Rev. 30 (2009) 19–34.

[185] S.B. Breitkopf, J.M. Asara, Determining in vivo phosphorylation sites using mass spectrometry, Curr. Protoc. Mol. Biol. Chapter 2012. https://doi.org/10.1002/0471142727.mb1819s98.

[186] M. Feric, B. Zhao, J.D. Hoffert, et al., Large-scale phosphoproteomic analysis of membrane proteins in renal proximal and distal tubule, Am. J. Physiol. Cell Physiol. 300 (2011) C755–C770.

[187] R.L. Gundry, M.Y. White, C.I. Murray, et al., Preparation of proteins and peptides for mass spectrometry analysis in a bottom-up proteomics workflow, Curr. Protoc. Mol. Biol. Chapter 2009. https://doi.org/10.1002/0471142727.mb1025s88.

[188] C. Richardson, K. Sakamoto, P. de los Heros, et al., Regulation of the NKCC2 ion cotransporter by SPAK-OSR1-dependent and -independent pathways, J. Cell Sci. 124 (2011) 789–800.

[189] R. Gunaratne, D.W. Braucht, M.M. Rinschen, et al., Quantitative phosphoproteomic analysis reveals cAMP/vasopressin-dependent signaling pathways in native renal thick ascending limb cells, Proc. Natl. Acad. Sci. U S A 107 (2010) 15653–15658.

[190] A.C. Vitari, J. Thastrup, F.H. Rafiqi, et al., Functional interactions of the SPAK/OSR1 kinases with their upstream activator WNK1 and downstream substrate NKCC1, Biochem. J. 397 (2006) 223–231.

[191] B. Sid, L. Miranda, D. Vertommen, et al., Stimulation of human and mouse erythrocyte Na$^+$-K$^+$-2Cl$^-$ cotransport by osmotic shrinkage does not involve AMP-activated protein kinase, but is associated with STE20/SPS1-related proline/alanine-rich kinase activation, J. Physiol. 588 (2010) 2315–2328.

[192] J.L. Smalley, G. Kontou, C. Choi, et al., Isolation and characterization of multi-protein complexes enriched in the K-Cl co-transporter 2 from brain plasma membranes, Front. Mol. Neurosci. 13 (2020), 563091.

[193] J. Rinehart, Y.D. Maksimova, J.E. Tanis, et al., Sites of regulated phosphorylation that control K-Cl cotransporter activity, Cell 138 (2009) 525–536.

[194] Z. Melo, P. de los Heros, S. Cruz-Rangel, et al., N-terminal serine dephosphorylation is required for KCC3 cotransporter full activation by cell swelling, J. Biol. Chem. 288 (2013) 31468–31476.

[195] A.N. Anselmo, S. Earnest, W. Chen, et al., WNK1 and OSR1 regulate the Na$^+$, K$^+$, 2Cl$^-$ cotransporter in HeLa cells, Proc. Natl. Acad. Sci. U S A 103 (2006) 10883–10888.

[196] A. Zagórska, E. Pozo-Guisado, J. Boudeau, et al., Regulation of activity and localization of the WNK1 protein kinase by hyperosmotic stress, J. Cell Biol. 176 (2007) 89–100.

[197] D. Lagnaz, J.P. Arroyo, M. Chávez-Canales, et al., WNK3 abrogates the NEDD4-2-mediated inhibition of the renal Na$^+$-Cl$^-$ cotransporter, Am. J. Physiol. Renal Physiol. 307 (2014) F275–F286.

[198] J. Zhang, G. Gao, G. Begum, et al., Functional kinomics establishes a critical node of volume-sensitive cation-Cl$^-$ cotransporter regulation in the mammalian brain, Sci. Rep. 6 (2016), 35986.

[199] K. Johansen, L. Svensson, Immunoprecipitation, Methods Mol. Med. 13 (1998) 15–28.

[200] L.C. Conway, R.A. Cardarelli, Y.E. Moore, et al., N-Ethylmaleimide increases KCC2 cotransporter activity by modulating transporter phosphorylation, J. Biol. Chem. 292 (2017) 21253–21263.

[201] T. Mahmood, P.-C. Yang, Western blot: Technique, theory, and trouble shooting, N. Am. J. Med. Sci. 4 (2012) 429–434.

[202] J.D. Klein, W.C. O'Neill, Volume-sensitive myosin phosphorylation in vascular endothelial cells: Correlation with Na-K-2Cl cotransport, Am. J. Physiol. 269 (1995) C1524–C1531.

[203] J.B. Matthews, J.A. Smith, K.J. Tally, et al., Na-K-2Cl cotransport in intestinal epithelial cells. Influence of chloride efflux and F-actin on regulation of cotransporter activity and bumetanide binding, J. Biol. Chem. 269 (1994) 15703–15709.

[204] J. Liu, X. Ma, G.F. Cooper, et al., Explicit representation of protein activity states significantly improves causal discovery of protein phosphorylation networks, BMC Bioinformatics 21 (2020), 379.

[205] A. Hannemann, P.W. Flatman, Phosphorylation and transport in the Na-K-2Cl cotransporters, NKCC1 and NKCC2A, compared in HEK-293 cells, PLoS One 6 (2011), e17992.

[206] A. Hannemann, J.K. Christie, P.W. Flatman, Functional expression of the Na-K-2Cl cotransporter NKCC2 in mammalian cells fails to confirm the dominant-negative effect of the AF splice variant, J. Biol. Chem. 284 (2009) 35348–35358.

[207] P. Blaesse, I. Guillemin, J. Schindler, et al., Oligomerization of KCC2 correlates with development of inhibitory neurotransmission, J. Neurosci. 26 (2006) 10407–10419.

[208] M.A. Virtanen, P. Uvarov, M. Mavrovic, et al., The multifaceted roles of KCC2 in cortical development, Trends Neurosci. 44 (2021) 378–392.

[209] P. Friedel, A. Ludwig, C. Pellegrino, et al., A novel view on the role of intracellular tails in surface delivery of the potassium-chloride cotransporter KCC2, eNeuro 2017. https://doi.org/10.1523/ENEURO.0055-17.2017.

[210] S.S. Josiah, N.F. Meor Azlan, A. Oguro-Ando, et al., Study of the functions and activities of neuronal K-Cl co-transporter KCC2 using western blotting, J. Vis. Exp. 2022. https://doi.org/10.3791/64179.

[211] A.J. Miller, Ion-selective microelectrodes for measurement of intracellular ion concentrations, Methods Cell Biol. 49 (1995) 275–291.

[212] R.D. Keynes, Chloride in the squid giant axon, J. Physiol. 169 (1963) 690–705.

[213] A. Strickholm, B.G. Wallin, Intracellular chloride activity of crayfish giant axons, Nature 208 (1965) 790–791.

[214] T.O. Neild, R.C. Thomas, Intracellular chloride activity and the effects of acetylcholine in snail neurones, J. Physiol. 242 (1974) 453–470.

[215] J.L. Walker Jr, Ion specific liquid ion exchanger microelectrodes, Anal. Chem. 43 (1971) 89A–93A.

[216] P. Bregestovski, T. Waseem, M. Mukhtarov, Genetically encoded optical sensors for monitoring of intracellular chloride and chloride-selective channel activity, Front. Mol. Neurosci. 2 (2009), 15.

[217] A.A. Vereninov, A.A. Rubashkin, T.S. Goryachaya, et al., Pump and channel K (Rb$^+$) fluxes in apoptosis of human lymphoid cell line U937, Cell. Physiol. Biochem. 22 (2008) 187–194.

[218] A. Ludwig, C. Rivera, P. Uvarov, A noninvasive optical approach for assessing chloride extrusion activity of the K-Cl cotransporter KCC2 in neuronal cells, BMC Neurosci. 18 (2017), 23.

[219] V.E. Yurinskaya, I.A. Vereninov, A.A. Vereninov, A tool for computation of changes in Na$^+$, K$^+$, Cl$^-$ channels and transporters due to apoptosis by data on cell ion and water content alteration, Front. Cell Dev. Biol. 7 (2019), 58.

[220] Y. Kovalchuk, O. Garaschuk, Two-photon chloride imaging using MQAE in vitro and in vivo, Cold Spring Harb. Protoc. 2012 (2012) 778–785.

[221] M. Engels, M. Kalia, S. Rahmati, et al., Glial chloride homeostasis under transient ischemic stress, Front. Cell. Neurosci. 15 (2021), 735300.

[222] S.H. Park, I. Shin, Y.H. Kim, et al., Mitochondrial Cl$^-$-selective fluorescent probe for biological applications, Anal. Chem. 92 (2020) 12116–12119.

[223] A. Savardi, M. Borgogno, R. Narducci, et al., Discovery of a small molecule drug candidate for selective NKCC1 inhibition in brain disorders, Chem 6 (2020) 2073–2096.

[224] V.I. Dzhala, D.M. Talos, D.A. Sdrulla, et al., NKCC1 transporter facilitates seizures in the developing brain, Nat. Med. 11 (2005) 1205–1213.

[225] I. Chamma, M. Heubl, Q. Chevy, et al., Activity-dependent regulation of the K/Cl transporter KCC2 membrane diffusion, clustering, and function in hippocampal neurons, J. Neurosci. 33 (2013) 15488–15503.

[226] M.A. Valdez-Flores, R. Vargas-Poussou, S. Verkaart, et al., Functionomics of NCC mutations in Gitelman syndrome using a novel mammalian cell-based activity assay, Am. J. Physiol. Renal Physiol. 311 (2016) F1159–F1167.

[227] M. Gagnon, M.J. Bergeron, G. Lavertu, et al., Chloride extrusion enhancers as novel therapeutics for neurological diseases, Nat. Med. 19 (2013) 1524–1528.

[228] D. Ponomareva, E. Petukhova, P. Bregestovski, Simultaneous monitoring of pH and chloride (Cl$^-$) in brain slices of transgenic mice, Int. J. Mol. Sci. 22 (2021), 13601.

[229] M. Davidov, N. Kakaviatos, F.A. Finnerty Jr, Antihypertensive properties of furosemide, Circulation 36 (1967) 125–135.

[230] M.J. Asbury, P.B. Gatenby, S. O'Sullivan, et al., Bumetanide: Potent new "loop"

diuretic, Br. Med. J. 1 (1972) 211–213.

[231] S.N. Orlov, S.V. Koltsova, L.V. Kapilevich, et al., NKCC1 and NKCC2: The pathogenetic role of cation-chloride cotransporters in hypertension, Genes Dis. 2 (2015) 186–196.

[232] P. Hampel, K. Römermann, N. MacAulay, et al., Azosemide is more potent than bumetanide and various other loop diuretics to inhibit the sodium-potassium-chloride-cotransporter human variants hNKCC1A and hNKCC1B, Sci. Rep. 8 (2018), 9877.

[233] A. Savardi, A. Patricelli Malizia, M. De Vivo, et al., Preclinical development of the Na-K-2Cl co-transporter-1 (NKCC1) inhibitor ARN23746 for the treatment of neurodevelopmental disorders, ACS Pharmacol. Transl. Sci. 6 (2023) 1–11.

[234] C. Pégurier, N. Bosman, P. Collart, et al., Benzyl prolinate derivatives as novel selective KCC2 blockers, Bioorg. Med. Chem. Lett. 20 (2010) 2542–2545.

[235] R.A. Deisz, S. Wierschke, U.C. Schneider, et al., Effects of VU0240551, a novel KCC2 antagonist, and DIDS on chloride homeostasis of neocortical neurons from rats and humans, Neuroscience 277 (2014) 831–841.

[236] R.P. Garay, C. Nazaret, P.A. Hannaert, et al., Demonstration of a [K⁺,Cl⁻]-cotransport system in human red cells by its sensitivity to [(dihydroindenyl) oxy]alkanoic acids: Regulation of cell swelling and distinction from the bumetanide-sensitive [Na⁺,K⁺,Cl⁻]-cotransport system, Mol. Pharmacol. 33 (1988) 696–701.

[237] R. Jarvis, S.F. Josephine Ng, A.J. Nathanson, et al., Direct activation of KCC2 arrests benzodiazepine refractory status epilepticus and limits the subsequent neuronal injury in mice, Cell Rep. Med. 4 (2023), 100957.

[238] L. Luo, J. Wang, D. Ding, et al., Role of NKCC1 activity in glioma K⁺ homeostasis and cell growth: New insights with the bumetanide-derivative STS66, Front. Physiol. 11 (2020), 911.

[239] F. Ferrini, L.E. Lorenzo, A.G. Godin, et al., Enhancing KCC2 function counteracts morphine-induced hyperalgesia, Sci. Rep. 7 (2017), 3870.

[240] I. Ferando, G.C. Faas, I. Mody, Diminished KCC2 confounds synapse specificity of LTP during senescence, Nat. Neurosci. 19 (2016) 1197–1200.

[241] E. Delpire, A. Baranczak, A.G. Waterson, et al., Further optimization of the K-Cl cotransporter KCC2 antagonist ML077: Development of a highly selective and more potent *in vitro* probe, Bioorg. Med. Chem. Lett. 22 (2012) 4532–4535.

[242] P.K. Lauf, A.A. Chimote, N.C. Adragna, Lithium fluxes indicate presence of Na-Cl cotransport (NCC) in human lens epithelial cells, Cell. Physiol. Biochem. 21 (2008) 335–346.

[243] M. Borgogno, A. Savardi, J. Manigrasso, et al., Design, synthesis, *in vitro* and *in vivo* characterization of selective NKCC1 inhibitors for the treatment of core symptoms in Down syndrome, J. Med. Chem. 64 (2021) 10203–10229.

[244] E.D. Freis, A. Wanko, I.M. Wilson, et al., Treatment of essential hypertension with chlorothiazide (diuril); its use alone and combined with other antihypertensive agents, J. Am. Med. Assoc. 166 (1958) 137–140.

[245] M. Moser, A.I. Macaulay, Chlorothiazide as an adjunct in the treatment of essential hypertension, Am. J. Cardiol. 3 (1959) 214–219.

[246] M.E. Ernst, M. Moser, Use of diuretics in patients with hypertension, N. Engl. J. Med. 361 (2009) 2153–2164.

[247] N.T. Pham, J.G. Owen, N. Singh, et al., The use of thiazide diuretics for the treatment of hypertension in patients with advanced chronic kidney disease, Cardiol. Rev. 31 (2023) 99–107.

[248] A.D. Hughes, How do thiazide and thiazide-like diuretics lower blood pressure? J. Renin Angiotensin Aldosterone Syst. 5 (2004) 155–160.

[249] D.H. Ellison, J. Loffing, Thiazide effects and adverse effects: Insights from molecular genetics, Hypertension 54 (2009) 196–202.

[250] M.B. Sandberg, A.D. Riquier, K. Pihakaski-Maunsbach, et al., ANG II provokes acute trafficking of distal tubule Na⁺-Cl⁻ cotransporter to apical membrane, Am. J. Physiol. Renal Physiol. 293 (2007) F662–F669.

[251] H. Velázquez, F.S. Wright, Effects of diuretic drugs on Na, Cl, and K transport by rat renal distal tubule, Am. J. Physiol. 250 (1986) F1013–F1023.

[252] E. Schlatter, R. Greger, C. Weidtke, Effect of "high ceiling" diuretics on active salt transport in the cortical thick ascending limb of Henle's loop of rabbit kidney. Correlation of chemical structure and inhibitory potency, Pflugers Arch. 396 (1983) 210–217.

[253] P.W. Feit, Aminobenzoic acid diuretics. 2,4-Substituted-3-amino-5-sulfamylbenzoic acid derivatives, J. Med. Chem. 14 (1971) 432–439.

[254] O.B. Tvaermose Nielsen, P.W. Feit, Structure-activity relationships of aminobenzoic acid diuretics and related compounds. E.J. Cragoe Jr, Diuretic Agents, Vol. 83, American Chemical Society, Washington, D.C., 1978, pp. 12–23.

[255] P.W. Feit, Bumetanide: Historical background, taxonomy and chemistry. A.F. Lant, Bumetanid, Marius Press, Camforth, 1990, pp. 1–13.

[256] M. Cohen, Pharmacology of bumetanide, J. Clin. Pharmacol. 21 (1981) 537–542.

[257] R.A. Frizzell, M. Field, S.G. Schultz, Sodium-coupled chloride transport by epithelial tissues, Am. J. Physiol. 236 (1979) F1–F8.

[258] H.C. Palfrey, P.W. Feit, P. Greengard, cAMP-stimulated cation cotransport in avian erythrocytes: Inhibition by "loop" diuretics, Am. J. Physiol. 238 (1980) C139–C148.

[259] P.W. Flatman, J. Creanor, Regulation of Na⁺-K⁺-2Cl⁻ cotransport by protein phosphorylation in ferret erythrocytes, J. Physiol. 517 (Pt 3) (1999) 699–708.

[260] K. Lykke, K. Töllner, K. Römermann, et al., Structure-activity relationships of bumetanide derivatives: Correlation between diuretic activity in dogs and inhibition of human NKCC2A transporter, Br. J. Pharmacol. 172 (2015) 4469–4480.

[261] T. Blauwblomme, V. Dzhala, K. Staley, Transient ischemia facilitates neuronal chloride accumulation and severity of seizures, Ann. Clin. Transl. Neurol. 5 (2018) 1048–1061.

[262] V.I. Dzhala, A.C. Brumback, K.J. Staley, Bumetanide enhances phenobarbital efficacy in a neonatal seizure model, Ann. Neurol. 63 (2008) 222–235.

[263] E. Lemonnier, Y. Ben-Ari, The diuretic bumetanide decreases autistic behaviour in five infants treated during 3 months with no side effects, Acta Paediatr. 99 (2010) 1885–1888.

[264] E. Lemonnier, C. Degrez, M. Phelep, et al., A randomised controlled trial of bumetanide in the treatment of autism in children, Transl. Psychiatry 2 (2012), e202.

[265] J.S. Soul, A.M. Bergin, C. Stopp, et al., A pilot randomized, controlled, double-blind trial of bumetanide to treat neonatal seizures, Ann. Neurol. 89 (2021) 327–340.

[266] J.J. Sprengers, D.M. van Andel, N.P.A. Zuithoff, et al., Bumetanide for core symptoms of autism spectrum disorder (BAMBI): A single center, double-blinded, participant-randomized, placebo-controlled, phase-2 superiority trial, J. Am. Acad. Child Adolesc. Psychiatry 60 (2021) 865–876.

[267] K. Töllner, C. Brandt, M. Töpfer, et al., A novel prodrug-based strategy to increase effects of bumetanide in epilepsy, Ann. Neurol. 75 (2014) 550–562.

[268] C. Brandt, P. Seja, K. Töllner, et al., Bumepamine, a brain-permeant benzylamine derivative of bumetanide, does not inhibit NKCC1 but is more potent to enhance phenobarbital's anti-seizure efficacy, Neuropharmacology 143 (2018) 186–204.

[269] H. Huang, M.I.H. Bhuiyan, T. Jiang, et al., A novel Na⁺-K⁺-Cl⁻ cotransporter 1 inhibitor STS66* reduces brain damage in mice after ischemic stroke, Stroke 50 (2019) 1021–1025.

[270] B. Welzel, R. Schmidt, L. Kirchhoff, et al., The loop diuretic torasemide but not azosemide potentiates the anti-seizure and disease-modifying effects of midazolam in a rat model of birth asphyxia, Epilepsy Behav. 139 (2023), 109057.

[271] K. Sturm, W. Siedel, R. Weyer, Inventors; Sulphamoylanthranilic acids, FRG patent 1,122,541 (CA 56:14032-33), 1962.

[272] K. Strange, T.D. Singer, R. Morrison, et al., Dependence of KCC2 K-Cl cotransporter activity on a conserved carboxy terminus tyrosine residue, Am. J. Physiol. Cell Physiol. 279 (2000) C860–C867.

[273] N.C. Adragna, M. Di Fulvio, P.K. Lauf, Regulation of K-Cl cotransport: From function to genes, J. Membr. Biol. 201 (2004) 109–137.

[274] E.R. Korpi, T. Kuner, P.H. Seeburg, et al., Selective antagonist for the cerebellar granule cell-specific gamma-aminobutyric acid type A receptor, Mol. Pharmacol. 47 (1995) 283–289.

[275] K.H. Reid, S.Z. Guo, V.G. Iyer, Agents which block potassium-chloride cotransport prevent sound-triggered seizures in post-ischemic audiogenic seizure-prone rats, Brain Res. 864 (2000) 134–137.

[276] L. Chen, J. Yu, L. Wan, et al., Furosemide prevents membrane KCC2 down-regulation during convulsant stimulation in the hippocampus, IBRO Neurosci. Rep. 12 (2022) 355–365.

[277] H.H. Lee, J.A. Walker, J.R. Williams, et al., Direct protein kinase C-dependent phosphorylation regulates the cell surface stability and activity of the potassium chloride cotransporter KCC2, J. Biol. Chem. 282 (2007) 29777–29784.

[278] Y.-T. Sun, C.-C. Shieh, E. Delpire, et al., K⁺-Cl⁻ cotransport mediates the bactericidal activity of neutrophils by regulating NADPH oxidase activation, J. Physiol. 590 (2012) 3231–3243.

[279] J. Zhang, X. Deng, K.T. Kahle, Leveraging unique structural characteristics of WNK kinases to achieve therapeutic inhibition, Sci. Signal. 9 (2016), e3.

[280] J. Lepault, F.P. Booy, J. Dubochet, Electron microscopy of frozen biological suspensions, J. Microsc. 129 (1983) 89–102.

[281] A. Assaiya, A.P. Burada, S. Dhingra, et al., An overview of the recent advances in cryo-electron microscopy for life sciences, Emerg. Top. Life Sci. 5 (2021) 151–168.

[282] D. Cressey, E. Callaway, Cryo-electron microscopy wins chemistry Nobel, Nature 550 (2017) 167.

[283] Y. Zhao, K. Roy, P. Vidossich, et al., Structural basis for inhibition of the Cation-chloride cotransporter NKCC1 by the diuretic drug bumetanide, Nat. Commun. 13 (2022), 2747.

[284] Y. Zhao, J. Shen, Q. Wang, et al., Structure of the human cation-chloride cotransport KCC1 in an outward-open state, Proc. Natl. Acad. Sci. U S A 119 (2022), e2109083119.

[285] X. Yang, Q. Wang, E. Cao, Structure of the human cation-chloride cotransporter NKCC1 determined by single-particle electron cryo-microscopy, Nat. Commun. 11 (2020), 1016.

[286] J.-H. Zhang, T.D. Chung, K.R. Oldenburg, A simple statistical parameter for use in evaluation and validation of high throughput screening assays, J. Biomol. Screen. 4 (1999) 67–73.

[287] P.M. Klein, A.C. Lu, M.E. Harper, et al., Tenuous inhibitory GABAergic signaling in the reticular thalamus, J. Neurosci. 38 (2018) 1232–1248.

[288] S. Sivakumaran, R.A. Cardarelli, J. Maguire, et al., Selective inhibition of KCC2 leads to hyperexcitability and epileptiform discharges in hippocampal slices and *in vivo*, J. Neurosci. 35 (2015) 8291–8296.

[289] Y.H. Raol, S.M. Joksimovic, D. Sampath, et al., The role of KCC2 in hyperexcitability of the neonatal brain, Neurosci. Lett. 738 (2020), 135324.

[290] F.J. Prael Iii, K. Kim, Y. Du, et al., Discovery of small molecule KCC2 potentiators which attenuate *in vitro* seizure-like activity in cultured neurons, Front. Cell Dev. Biol. 10 (2022), 912812.

[291] J.S. Grimley, L. Li, W. Wang, et al., Visualization of synaptic inhibition with an optogenetic sensor developed by cell-free protein engineering automation, J. Neurosci. 33 (2013) 16297–16309.

[292] S. Gill, R. Gill, Y. Wen, et al., A high-throughput screening assay for NKCC1 cotransporter using nonradioactive rubidium flux technology, Assay Drug Dev. Technol. 15 (2017) 167–177.

[293] A.S. Roy, M.S.S. Sawrav, M.S. Hossain, et al., *In silico* identification of potential inhibitors with higher potency than bumetanide targeting NKCC1: An important ion co-transporter to treat neurological disorders, Inform. Med. Unlocked 27 (2021), 100777.